Scientific Research Publishing

Open Journal of Modern Hydrology, 2026, 16(2), 177-212
https://www.scirp.org/journal/ojmh
ISSN Online: 2163-0496
ISSN Print: 2163-0461

Analysis of Climate Trends from 1981 to 2050 for Precipitation and Temperatures in the Mouhoun Watershed (Samandeni, Burkina Faso) Based on CMIP6 Simulations Corrected Using NEX-GDDP

Dioviel Dominique Somda[1], Ali Doumounia[1,2], Wenceslas Somda[1,3], Moumouni Djibo[1,4], Telado Luc Bambara[1,2], François Zougmore[1]

[1]Laboratory of Materials and Environment, Université Joseph Ki-Zerbo, Ouagadougou, Burkina Faso
[2]Institute of Science and Technology, Ecole Normale Supérieure Ouagadougou, Burkina Faso
[3]Université Daniel Ouezzin Coulibaly, Dédougou, Burkina Faso
[4]Université Virtuelle, Ouagadougou, Burkina Faso
Email: doumouniaali@yahoo.fr

How to cite this paper: Somda, D.D., Doumounia, A., Somda, W., Djibo, M., Bambara, T.L. and Zougmore, F. (2026) Analysis of Climate Trends from 1981 to 2050 for Precipitation and Temperatures in the Mouhoun Watershed (Samandeni, Burkina Faso) Based on CMIP6 Simulations Corrected Using NEX-GDDP. *Open Journal of Modern Hydrology*, **16**, 177-212.
https://doi.org/10.4236/ojmh.2026.162011

Received: November 21, 2025
Accepted: March 13, 2026
Published: March 16, 2026

Abstract

In the Sahelian context, characterized by high climate variability, this study aims to produce reliable, high-resolution climate information that can be directly used by climate services to support decision-making in agriculture, water management and climate risk reduction in Burkina Faso. Changes in precipitation and temperatures are analyzed over the period 1981-2050 using local observation data and CMIP6 projections from NEX-GDDP, corrected for bias using Quantile Mapping. Trends are assessed using the Mann-Kendall test, their amplitude estimated using the Theil-Sen estimator, and breaks detected using the Pettitt test. The analysis is based on future climate normals (2001-2030, 2011-2040 and 2021-2050) and includes extreme indices relevant to sectoral uses, such as the duration of consecutive dry and wet sequences (CDD and CWD), average daily rainfall intensity (SDII) and maximum daily precipitation (RX1day). The results show a gradual increase in annual precipitation: +2.86 mm/year over the historical period, +4.53 mm/year under SSP2-4.5 and +5.56 mm/year under SSP5-8.5, accompanied by a continuous rise in average temperatures (0.024˚C/year over 1981-2014, then 0.02˚C/year and 0.046˚C/year according to future scenarios), all of which are significant trends ($p < 0.05$). Major disruptions appear around 1995 for the for historical data and 2031-2032 for projections. The intensification of daily rainfall and the re-

duction in dry and wet sequences reflect increased intra-seasonal variability. These results provide a solid scientific basis for agricultural planning, optimization of water infrastructure and anticipation of hydrometeorological risks, reinforcing adaptation strategies in response to rapid climate change in the Sahel, particularly in the Mouhoun basin in Samandeni.

Keywords

Climate Change, Extreme Precipitation, Future Temperatures, Hydrometeorological Risks, Agricultural Adaptation

1. Introduction

Climate change is one of the major challenges facing humanity today. It is a widely recognized global phenomenon whose impacts vary from region to region [1]. The IPCC's 6th Assessment Report shows that West Africa is among the regions experiencing the most rapid warming, leading to more frequent heat waves, prolonged dry seasons, increased evapotranspiration, and amplified rainfall variability [2] [3]. These changes have a direct impact on food security, rain-fed agriculture, ecosystems, energy, and water resources. Furthermore, [4] states that many countries will be affected by temperature increases, which will have serious repercussions on the agricultural systems of countries that depend solely on rainfall. Since the 1970s, the Sahel region has experienced marked fluctuations between periods of drought and phases of relative recovery in rainfall [5] [6]. Burkina Faso, like the rest of West Africa, is experiencing alternating years of rainfall deficits and surpluses and a continuous rise in temperatures [5]. This change in climate, identified by changes in temperature and precipitation, affects the hydrology of watersheds [7] and, consequently, the availability of water resources on a spatial and temporal scale.

There is a wealth of literature on the climate in the Sahelian zone, but most studies have not taken into account rainfall distribution according to climate zones [8]. The high degree of climate variability highlights the value of analyses conducted at the watershed level. It therefore seems appropriate to study climate change not only at the level of different climate zones, but even more so at the level of watersheds. According to [9], new hydro-climatic disasters, namely water shortages in the form of droughts, are to be expected, as they could affect countries' economies and food security. In addition, global average temperature projections predict a 1.5˚C increase in temperature by 2050. Knowledge of current and future trends in climate variables is therefore crucial for better decision-making.

The aim of this article is to analyze past and future trends in precipitation and average annual temperatures, to analyze the evolution of future climate norms in relation to the 1991-2020 climate norm, and finally to analyze the trends of some climate indices in order to identify the likely climate risks in the watershed. Burkina Faso is characterized by three (03) constantly changing climatic zones

described by different normals, the most recent of which is 1991-2020. In the literature, there are very few studies on the evolution of climatic parameters in the study area. However, at the scale of the Sudanese phytogeographic domain, a few studies have been carried out by authors such as who analyzed trends in climate variability and extremes in the Sudanese domain in western Burkina Faso, or again [10] who conducted studies on the intensification of climate risks to cotton cultivation. These studies show that average annual rainfall and temperatures over the period 1991-2020 are on the rise in this area. Studying climate change is very important for ensuring better resource planning. To study the future climate, it is necessary to use projection data, which is now essential for modeling future conditions in order to understand past and future challenges. High-resolution data such as that from NASA's NEX-GDDP program, based on CMIP6 models, provides an opportunity to analyze recent climate trends in detail. However, these data require correction for systematic biases in the models, justifying the use of techniques such as Quantile Mapping [11]. This study, therefore, contributes to our understanding of the climate of the Mouhoun watershed in Samandeni.

2. Data and Methodology

2.1. Study Area

The Mouhoun watershed in Samandeni is located between 4˚43' and 5˚35' west longitude and 10˚7' and 11˚7' north latitude. It covers an area of 4418.62 km^2 and contributes to the water supply of the Samandeni dam, located downstream (**Figure 1**).

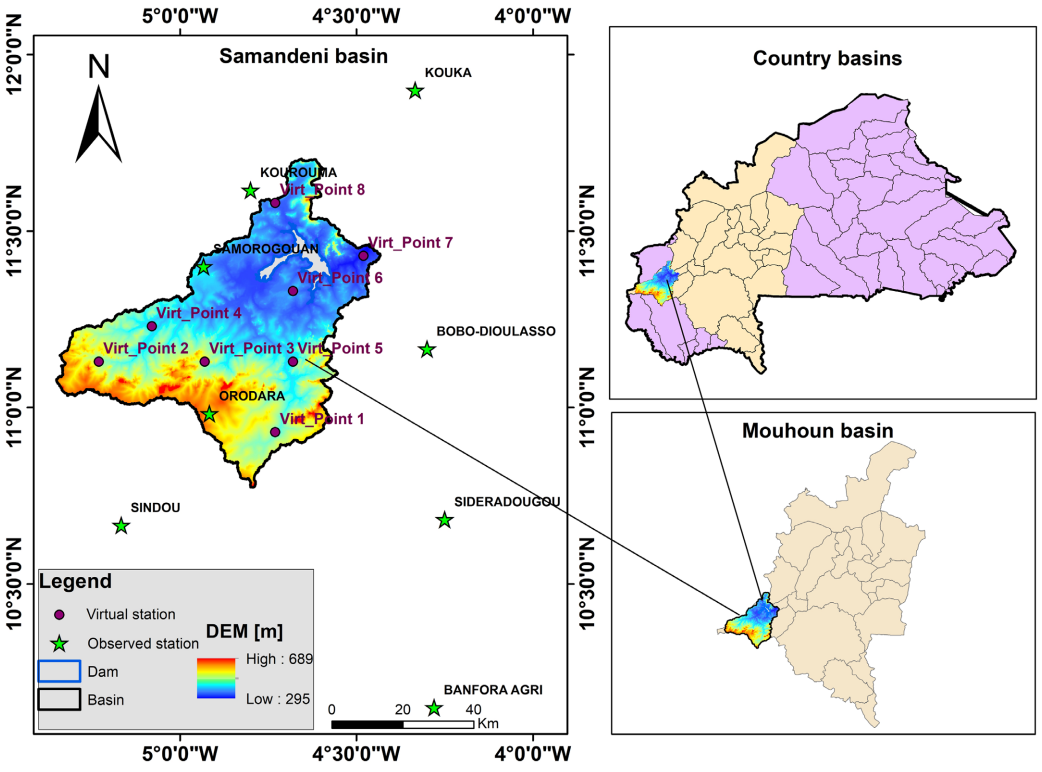

Figure 1. Mouhoun watershed at the Samandeni hydrometric station.

It is located in a typical Sudanese climate zone and peaks at 686 m with two (02) seasons: a dry season from November to May and a rainy season from June to October, where the average annual rainfall varies between 900 and 1200 mm [8]. Over the period 1981-2014, maximum temperatures reached 42˚C in April and minimum temperatures reached 10˚C in January.

2.2. Study Data

2.2.1. Observed Data

The observation climate data used in this study comes from synoptic and agroclimatic stations located throughout Burkina Faso. These stations are operated by the National Meteorological Agency of Burkina Faso (ANAM-BF). Rainfall data was collected from stations in Bobo-Dioulasso, Banfora, Kouka, Kourouma, Orodara, Samoroguan, and Sindou. Minimum and maximum temperature data was collected for the period from 1980 to 2024. This data was supplemented by merged data provided by the AGRHYMET Regional Center in Niamey. These data are derived from the fusion of CHIRPS data and observation data. Given the sparse distribution of weather stations in the watershed, spatial interpolation of the observed data at ground-based weather using the inverse distance weighting (IDW) method was used to extract data corresponding to eight (08) virtual stations located at grid points. The choice of precipitation and temperature for this analysis is explained by the fact that in sub-Saharan Africa, these data bests characterize the climate and its evolution [12].

2.2.2. GCM and Climate Projection Data

To improve knowledge about climate change and detect past, present, and future effects related to climate change, global climate models (GCMs) under the supervision of the Coupled Model Intercomparison Project (CMIP) have been established by groups of modelers around the world [13]. CMIP uses multiple models to better understand past, present, and future climate change caused by changes in radiative forcing or natural unforced variability [14]. Climate model data are accessible through the World Climate Research Program (WCRP), which oversees the various phases of CMIP [15]. The models in the IPCC's Sixth Assessment Report (AR6) projected climate variables and changes using a set of five new climate scenarios known as Shared Socioeconomic Pathways (SSPs), which are SSP1-1.9 (extremely low), SSP1-2.6 (low), SSP2-4.5 (moderate), SSP3-7.0 (high), and SSP5-8.5 (very high) [16] [17]. These scenarios make it possible to analyze and project various emission scenarios related to climate change. Version 6 of CMIP, which is the most recent, has proven its ability to reproduce climate change, although its coarse spatial resolution limits its application [18]. The use of high spatial resolution projection data (precipitation, temperature, wind, etc.) is therefore necessary to conduct studies on the impacts of climate change. Given the uncertainties associated with biases in climate models, it is recommended that more than ten climate models be used in studies of the impact of climate change on the hydrological cycle [19].

In this study, data from NASA Earth Exchange-Global Daily Downscaled Projections (NEX-GDDP) models were used to analyze precipitation and temperature trends across the Mouhoun watershed in Samandeni. These data, with a resolution of 0.25˚ × 0.25˚, or approximately 25 km × 25 km, are available via the NEX-GDDP-CMIP6 platform hosted by the NASA Center for Climate Simulation (NCCS) at https://ds.nccs.nasa.gov/thredds/catalog/AMES/NEX/GDDP-CMIP6/catalog.html. A total of twenty-seven (27) models (Table 1) were considered for this study.

Table 1. List of twenty-seven CMIP6 climate models from NEX-GDDP considered.

N˚	Models	Region	Variant
1	ACCESS-CM2	Australia	r1i1p1f1
2	ACCESS-ESM1-5	Australia	r1i1p1f1
3	CanESM5	Canada	r1i1p1f1
4	CMCC-CM2-SR5	Italy	r1i1p1f1
5	CMCC-ESM2	Italy	r1i1p1f1
6	CNRM-CM6-1	France	r1i1p1f2
7	CNRM-ESM2-1	France	r1i1p1f2
8	EC-Earth3-CC	Sweden	r1i1p1f1
9	EC-Earth3-veg-LR	Sweden	r1i1p1f1
10	FGOALS-g3	Chinese Mainland	r3i1p1f1
11	GFDL-ESM4	United States	r1i1p1f1
12	GISS-E2-1-G	United States	r1i1p1f2
13	HadGEM31-LL	United Kingdom	r1i1p1f3
14	INM-CM4-8	Rusia	r1i1p1f1
15	INM-CM5-0	Rusia	r1i1p1f1
16	IPSL-CM6A-LR	France	r1i1p1f1
17	KACE-1-0-G	Korea	r1i1p1f1
18	KIOST-ESM	Korea	r1i1p1f1
19	MIROC6	Japan	r1i1p1f1
20	MIROC-ES2L	Japan	r1i1p1f2
21	MPI-ESM1-2-HR	Germany	r1i1p1f1
22	MPI-ESM1-2-LR	Germany	r1i1p1f1
23	MRI-ESM2-0	Japan	r1i1p1f1
24	NorESM2-LM	Norway	r1i1p1f1
25	NorESM2-MM	Norway	r1i1p1f1
26	TaiESM1	Taiwan Region, China	r1i1p1f1
27	UKESM1-0-LL	United Kingdom	r1i1p1f1

2.3. Methodology

2.3.1. Models Performance

To ensure the reliability of the projections, the performance of the CMIP6 models was evaluated by comparing historical simulations with local observational data. Performance was assessed using Taylor's diagram based on a combination of metrics such as the correlation coefficient (R), which measures the temporal agreement between simulations and observations; the centered root mean square error ($RMSE_c$), which quantifies the dispersion of errors; and the standard deviation (sd), which measures the dispersion around the mean. The best model is the one with an sd close to the observed data, with a low $RMSE_c$ and a high R [20]. Let us assume two (02) sets of time series A and B of observation and simulation such that: $A=\{a_1,a_2,\cdots,a_n\}$ and $B=\{b_1,b_2,\cdots,b_n\}$ of n elements. The correlation coefficient (R) is given by Equation (1).

$$R=\frac{\sum_{i=1}^{n}\left(a_i-\bar{a}\right)\left(b_i-\bar{b}\right)}{\sqrt{\sum_{i=1}^{n}\left(a_i-\bar{a}\right)^2}\sqrt{\sum_{i=1}^{n}\left(b_i-\bar{b}\right)^2}}=\frac{\sum_{i=1}^{n}\left(a_i-\bar{a}\right)\left(b_i-\bar{b}\right)}{\sigma_a\sigma_b} \tag{1}$$

The standard deviations (σ) of the observed and simulated values are given by the equations:

$$\sigma_a=\sqrt{\frac{1}{n}\sum_{i=1}^{n}\left(a_i-\bar{a}\right)^2} \tag{2}$$

$$\sigma_b=\sqrt{\frac{1}{n}\sum_{i=1}^{n}\left(b_i-\bar{b}\right)^2} \tag{3}$$

The centered mean square error is given by the equation:

$$\mathrm{RMSE}_c=\sqrt{\frac{1}{n}\sum_{i=1}^{n}\left[\left(b_i-\bar{b}\right)-\left(a_i-\bar{a}\right)\right]^2} \tag{4}$$

Since 2001, the Taylor diagram has been widely used in hydroclimatic studies, with 6642 citations according to Web of Science (website consulted on December 22, 2025, at 2:14 a.m.). It is therefore a robust tool for identifying the best models. The Taylor diagram, based on a 2D space, is currently the most common method for evaluating model [21]-[24].

2.3.2. Bias Correction

There are various methods of bias correction in the literature (Delta, Linear Scaling, quantile mapping or quantile-quantile, CDFt, etc.). Among these, the Delta and quantile-quantile methods are the most commonly used [25]-[27]. To correct for systematic biases, the Quantile Mapping (QM) method was applied in this study. This method adjusts the distribution of simulated values to match that of local observations, while preserving the temporal variations of the model [11]. The process includes:

- extracting the cumulative distributions of observations and simulations,
- applying a quantile transformation to adjust the simulations,
- validating the corrected data by graphical and statistical comparison with ob-

servations.

This approach is known to improve the quality of climate projections at the regional level, particularly for extreme variables such as precipitation. A quantile of the simulated distribution is replaced by the same quantile of the observed distribution. Quantile mapping using a distribution involves transformations to adjust the distribution of the simulated variable P_m so that it matches the distribution of the observed variable P_o according to Equation (5) [28].

$$P_o = \mathrm{CDF}^{-1}\left(\mathrm{CDF}\left(P_m\right)\right) \tag{5}$$

where:

P_o : Observed variable,

P_m : Simulated variable,

CDF : Cumulative distribution function,

CDF^{-1} : Quantile function (inverse of CDF).

Once estimated, the correction function is applied to the variable derived from future climate simulations, which can ultimately be taken into account in socio-economic impact studies in the context of global change [27].

2.3.3. Data Series Trends

In this study, the Mann Kendall test was used to detect statistically significant trends in precipitation and temperature series. The purpose of the trend analysis is to detect and quantify climate change over the periods 1981-2014 and 2015-2020. The methodological steps are:

- Mann-Kendall (MK) test: a nonparametric test that detects monotonic trends in time series. The version adapted to autocorrelated series was used to limit false positives due to autocorrelation [29] [30],
- Sen slope: robust estimation of the magnitude of the trend for each climate variable, expressed per unit of time [31],
- Statistical significance: trends are considered significant if $p < 0.05$,
- Visualization: mapping of spatial trends and time series graphs to identify the most affected areas.

This combination of the MK test and Sen's slope allows for reliable analysis of climate trends, even with incomplete or noisy data, and provides a solid basis for projecting future impacts.

1) Mann-Kendall test

Trend analysis is considered as one of the most important topics in climate change studies [32]. According to [33] [34], this test using for trend detection is recommended by the World Meteorological Organization (WMO). In its implementation, the null hypothesis (H_0) assumes the absence of a monotonic trend in the time series, while the alternative hypothesis (H_1) assumes the presence of a monotonic trend in the data series.

For a sample of n supposed random and independent observation data points constituting a time series (x_1, x_2, …, x_n), the test statistic S is given by Equation (6):

$$S = \sum_{i=1}^{n-1} \sum_{j=i+1}^{n} \operatorname{sgn}\left(x_j - x_i\right) \tag{6}$$

where $j > i$ et

$i = 1, 2, 3, \cdots, n-1$ $j = 2, 3, 4, \cdots, n$ n : number of observation data.

$\operatorname{sgn}\left(x_j - x_i\right)$ is calculated according to equation 7:

$$\operatorname{sgn}\left(x_j - x_i\right) = \begin{cases} +1 & \text{if } x_j > x_i \\ 0 & \text{if } x_j = x_i \\ -1 & \text{if } x_j < x_i \end{cases} \tag{7}$$

Thus, a positive value of S indicates an upward trend, while a negative value indicates a downward trend in the time series of data. According to [29], S statistic calculated in this way is distributed asymptotically according to a normal distribution with mean zero and variance var(S) given by Equation (8) [17].

$$\operatorname{Var}(S) = \frac{1}{18}\left[n(n-1)(2n+5) - \sum_{p=1}^{k} t_p \left(t_p - 1\right)\left(2t_p + 5\right) \right] \tag{8}$$

where

p: the number of groups of identical values within the data;

t_p: the number of elements present in the p-th group of equality;

n: total number of observations constituting the time series.

In cases where the sample size $n \geq 30$, the standard normal test statistic Z_s is calculated using Equation (9).

$$Z_s = \begin{cases} \dfrac{S-1}{\sqrt{\operatorname{Var}(S)}} & \text{si } S > 0 \\ 0 & \text{si } S = 0 \\ \dfrac{S+1}{\sqrt{\operatorname{Var}(S)}} & \text{si } S < 0 \end{cases} \tag{9}$$

Z_s is used to determine the significance of the trend. It indicates the strength and direction of the trend. Thus, when Z_s is positive and significant, the trend is upward; when Z_s is negative and significant, the trend is downward [35]. Although the Mann-Kendall test is a robust test widely used by many authors [1] [36] [37] to detect the existence of a linear trend, it does not provide any indication of the magnitude of the trend. For this reason, we use Sen's estimator.

2) Theil-Sen estimator

[31] allows us to assess the magnitude of the trend in time series data. It uses a linear model to estimate the slope of the trend by calculating it from all possible pairwise comparisons of observation values, giving a total of N slopes with

$$N = \frac{n(n-1)}{2} \tag{10}$$

The equations used to estimate the slope a and the y-intercept b are as follows:

$$\alpha = \operatorname{median}\left(\frac{x_j - x_i}{t_j - t_i} \right) \tag{11}$$

$$\beta = x_i - \alpha \times t_i \quad \forall i = 1, 2, \cdots, n \tag{12}$$

where:

$x_j - x_i$: difference in observation values between two points in time,

$t_j - t_i$: time difference between two observations.

N: the total number of non-zero differences $t_j - t_i$ for all pairs (*i*, *j*) such that $1 \le i < j \le n$.

The Theil-Sen technique is robust to outliers, allowing it to ignore extreme values without affecting the overall estimate of the slope. It can reject up to approximately 29.28% of the sample size as outliers (known as the failure limit $(1-1/\sqrt{2})$) sans without compromising the result [35].

2.3.4. Homogeneity Test of Data

Where possible, the data used to calculate climatological norms and averages should be homogeneous [38]. Within the framework of this study, the non-parametric test was used. This test is widely used in the literature to detect a single change in the mean in a series of continuous data. Null hypothesis (H_0) assumes that there is no change in the mean of the data series, whereas alternative hypothesis (H_1) assumes that there is a change in the mean of the data series. The U statistic of the Pettitt test is given by:

$$U = \max \left| \sum_{i=1}^{n-1} \sum_{j=t+1}^{n} \operatorname{sgn}\left(x_t - x_j\right) \right| \tag{13}$$

where

$$\operatorname{sgn}\left(x_t - x_j\right) = \begin{cases} +1 & \text{si } x_t > x_j \\ 0 & \text{si } x_t = x_j \\ -1 & \text{si } x_t < x_j \end{cases} \tag{14}$$

Pettitt's test allows the main climate series of several elements to be divided into two climate sub-series, highlighting different statistical distributions separated by a break. A break occurs in a given year when U reaches its maximum value.

2.3.5. Climate Normal

The normal is a derivative of raw agro-climatic products. Calculating the normal is a good indicator for analyzing climate change. According to the WMO Technical Regulations, standard climatological normals are averages of climatological data calculated for consecutive 30-year periods [38]. Furthermore, the WMO recommends calculating anomalies, as far as possible, based on periods corresponding to standard climatological normals, in order to establish a uniform basis for comparison. The annual normal precipitation or temperature $y_{norm,an}$ over a given period is given by the following Equation (15):

$$y_{norm,an} = \frac{1}{N} \sum_{i}^{n} y_{ann,i} \tag{15}$$

with:

y_i: Total precipitation or average temperature recorded during year *i*, *N*: Num-

ber of years covering the reference period.

For the purposes of this study, the annual normal was considered and the latest normal in effect is that of 1991-2020.

2.3.6. Climate Extremes

Knowledge of a region's climate is very important for managing the weather phenomena that occur there, whether beneficial or harmful [39]. Given the spatial and temporal heterogeneity of climate change and extreme events, the Intergovernmental Panel on Climate Change (IPCC) has indicated that it is important to study climate change and extremes at the regional and local levels in order to better support the response of states and economic organizations to climate change [40]. To analyze extreme events, it is important to analyze climate indices. These indices represent an important impact parameter widely used in many disciplines, particularly when extreme events are taken into account. In this study, six (06) climate indices for precipitation and temperature (**Table 2**) were used out of the twenty-seven (27) climate indices recommended by the World Meteorological Organization's Expert Team on Climate Change Detection, Monitoring, and Indices. The 27 climate indices can be found at: https://etccdi.pacificclimate.org/list_27_indices.shtml (accessed on 12/08/2025 at 12:58 a.m.). Several authors such us [40]-[43] used these climate indices to study extreme events in West Africa.

Table 2. Definition of precipitation and temperature indices used in this study.

ID	Index names	Definition	Units
RX1day	Maximum precipitation in 1 day	Monthly maximum precipitation over 1 day mm	mm
SDII	Simple daily intensity index	Annual total precipitation on wet days divided by the number of wet days with RR ≥ 1 mm	mm/days
CWD	Consecutive wet days	Maximum number of consecutive days with RR ≥ 1 mm:	days
CDD	Consecutive dry days	Maximum number of consecutive days with RR < 1 mm	days
TXx	Maximum maximum temperatures	Monthly maximum value of daily maximum temperature	˚C
TNn	Minimum minimum temperatures	Monthly minimum value of daily minimum temperature	˚C

3. Results

3.1. Model Selection and Bias Correction

3.1.1. Inter-Model Uncertainties

Although CMIP6 models tend to represent the West African monsoon better than CMIP5 models, common systematic biases and high inter-model dispersion per-

sist, limiting the reliability of future climate projections in the region [19] [44]. Furthermore, the main uncertainty in projections of future climate change remains the sensitivity of global mean temperature to variations in the Earth's energy balance, commonly referred to as radiative forcing. This response is generally quantified using the equilibrium climate sensitivity (ECS), defined as the increase in global mean temperature associated with a doubling of atmospheric carbon dioxide concentration, for which the radiative forcing is relatively well known. It also takes into account the transient climate response (TCR) [45]. However, CMIP6 simulations show an overall increase in climate sensitivities in the new Earth system models, with more than a third of the models now showing ECS values above 4.5 K [46], and several models showing high transient climate response (TCR) values exceeding 2.5 K [45]. In order to quantify and illustrate this persistent dispersion between models, a detailed analysis of inter-model uncertainty was carried out over the reference period. This analysis highlights an average coefficient of variation greater than 2.36 over the reference period. This high level of relative variability is associated with an average inter-model standard deviation of 3.97 mm/day, which is higher than the estimated multi-model average of 2.83 mm/day. The results obtained indicate a significant dispersion of simulations around the multi-model average, reflecting a strong disagreement between models. This reveals the presence of both structural and relative uncertainties. Nevertheless, despite this overall dispersion, the analysis of position indicators shows good consensus among the majority of models, consistent with observations. In particular, the low interquartile range (IQR) values suggest that the central half of the models have simulations that are very close to each other, indicating robust agreement among the dominant models in the set.

3.1.2. Model Selection

Applying the Taylor diagram to the NEX-GDDP model data from the study identified CanESM5 as the model that best reproduces the climate in the Mouhoun basin in Samandeni. The model was selected based on a combination of several metrics (RMSE, R, and standard deviation), the results of which are shown in **Table 3**. The best model is the one with the smallest RMSE, a high correlation coefficient, and a low standard deviation ratio (RSD).

Table 3. Results of the metrics for the 27 climate models used in the Taylor diagram.

Models	RMSE	R	RSD	Rank
CanESM5	6.13	0.33	0.77	1
MIROC_ES2L	6.34	0.31	0.82	2
MPI_ESM1_2_LR	6.48	0.31	0.86	3
GISS_E2_1_G	6.49	0.29	0.84	4
ACCESS_ESM1_5	6.52	0.3	0.86	5
ACCESS_CM2	6.52	0.3	0.86	6

Continued

FGOALS_g3	6.54	0.27	0.83	7
CNRM_CM6_1	6.56	0.31	0.89	8
NorESM2_LM	6.57	0.31	0.89	9
MPI_ESM1_2_HR	6.64	0.3	0.9	10
IPSL_CM6A_LR	6.65	0.29	0.88	11
EC_Earth3	6.67	0.29	0.89	12
Earth3_Veg_LR	6.68	0.29	0.9	13
INM_CM4_8	6.68	0.28	0.88	14
INM_CM5_0	6.71	0.27	0.88	15
CNRM_ESM2_1	6.72	0.27	0.88	16
MIROC6	6.73	0.29	0.91	17
TaiESM1	6.76	0.29	0.92	18
MRI_ESM2_0	6.86	0.28	0.94	19
CMCC_CM2	6.89	0.25	0.91	20
CMCC_ESM2	6.96	0.26	0.94	21
GFDL_ESM4	6.99	0.25	0.94	22
NorESM2_MM	6.99	0.27	0.96	23
KIOST_ESM	7.66	0.1	0.93	24
HadGEM3_GC31_LL	8.14	-0.07	0.88	25
UKESM1_0_LL	8.14	-0.06	0.89	26
KACE_1_0_G	9.1	-0.09	1.08	27

3.1.3. Correction de Biais

Bias correction applied to the outputs of the CanESM5 model using the quantile–quantile method allowed the simulated climate series to be adjusted to the observations. This improvement is reflected in satisfactory performance scores, evaluated using the metrics in **Table 4**, in accordance with the methodological approach proposed by [47].

Table 4. Definition of precipitation and temperature indices used in this study.

Metrics	Raw GCM	Corrected GCM
Nash Sutcliff Efficiency (NSE)	−0.08	−0.47
Kling Gupta Efficiency (KGE)	0.30	0.28
d1	0.55	0.55
Kling Gupta Efficiency parametrique (KGE_p)	0.29	0.28
Kling Gupta Efficiency non paramétrique (KGE_np)	0.55	0.63
DE	0.09	0.08

Aside from the nonparametric Kling Gupta Efficiency (KGE_np), which gives a satisfactory score of 0.63 after correction compared to 0.55 before correction, the other metrics show low scores.

3.2. Precipitation and Temperature Trends

In this study, precipitation and average annual temperature were used. Annual precipitation totals are the most commonly used indicator for describing long-term rainfall trends [48]. The results of the trend analysis, using the Mann-Kendall test and Sen's estimator of rainfall and temperature data for both the reference period and the projection period, are showed in the following paragraphs.

Precipitation: over the reference period (1981-2014), the results show a statistically insignificant positive trend (p-value = 0.224, Z = 1.215) at a significance level of 5% in the average annual precipitation data for the Mouhoun watershed in Samandeni (**Figure 2**). This positive trend reflects an increase in precipitation of +2.86 mm/year in the watershed.

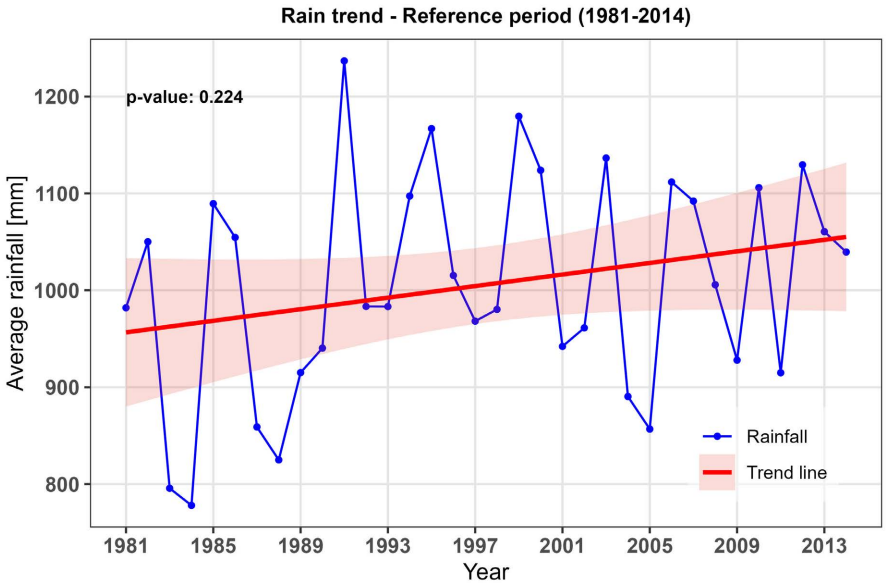

Figure 2. Trend in average annual rainfall (1981-2014).

However, over the projection period (2015-2050), the trends observed in precipitation are positive and significant (**Figure 3**), respectively for the SSP2-4.5 (p-value = 0.0067, Z = 2.71) and SSP5-8.5 (p-value = 0.0012, Z = 3.228). These positive trends reflect an increase in precipitation of +4.53 mm/year and +5.56 mm/year respectively at the watershed scale.

Temperature: The average annual temperature over the reference period (**Figure 4**) shows a statistically significant positive trend (p-value = 0.007, Z = 2.698). This positive trend is characterized by a temperature increase of +0.024˚C/year.

In contrast, over the projection period, analysis of average temperatures across the watershed indicates significant upward trends (p-value = 0.0001 and p-value = 1.59×10^{-9}) for the SSP2-4.5 and SSP5-8.5 emission scenarios, respectively

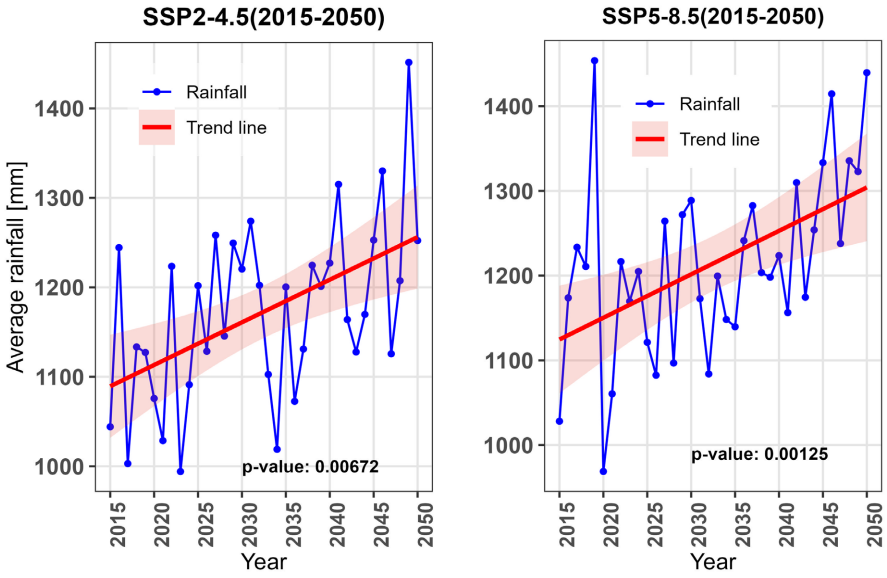

Figure 3. Average rainfall trend over the projection period (left: SSP2-4.5 scenario, right: SSP5-8.5 scenario).

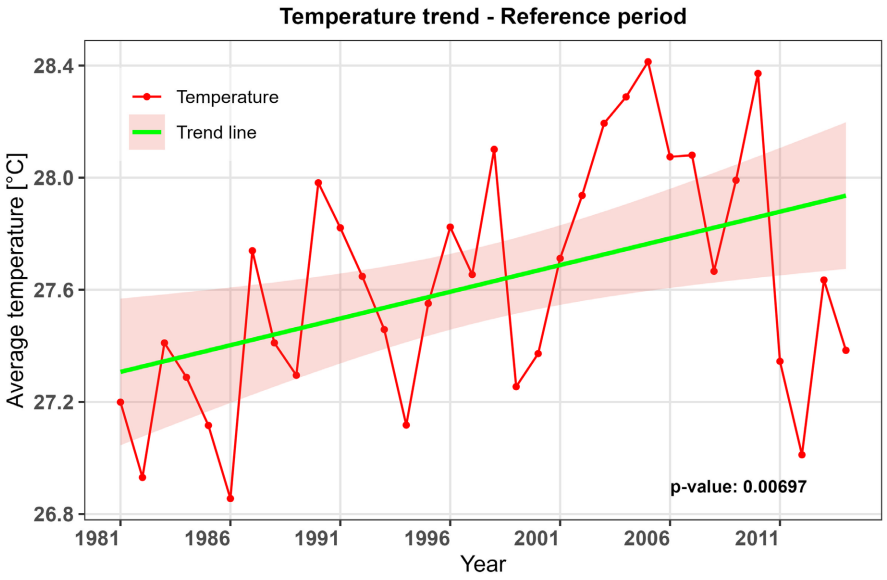

Figure 4. Trend in average temperature (1981-2014).

(**Figure 5**). These increases translate into a temperature rise of +0.02˚C/year and +0.046˚C/year at the basin scale, respectively.

The SSP2-4.5 and SSP5-8.5 scenarios predict a decrease in precipitation during the DJF and SON months. These scenarios also predict an increase in precipitation following the MAM and JJA months compared to the reference period. In terms of temperatures, the SSP2-4.5 scenarios predict a decrease in temperature during the DJF and MAM months and an increase in temperature during the JJA and SON months. The SSP5-8.5 scenario predicts an increase in temperature for all months of the year during the 2015-2050 period across the basin. On a seasonal basis, rainfall is expected to decrease by 1.41 mm/year and 0.97 mm/year accord-

ing to the SSP2-4.5 and SSP5-8.5 scenarios, respectively, during the SON season (Table 5), corresponding to a difference of 2.79 mm/year and 0.41 mm/year compared to the reference scenario. The JJA season remains the season with the most abundant rainfall in the basin. During this season, an increase of 4.43 mm/year is expected for SSP2-4.5 compared to 1.83 mm/year for SSP5-8.5, which translates into an increase of 3.83 mm/year and 1.43 mm/year for the SSP2-4.5 and SSP5-8.5 scenarios, respectively.

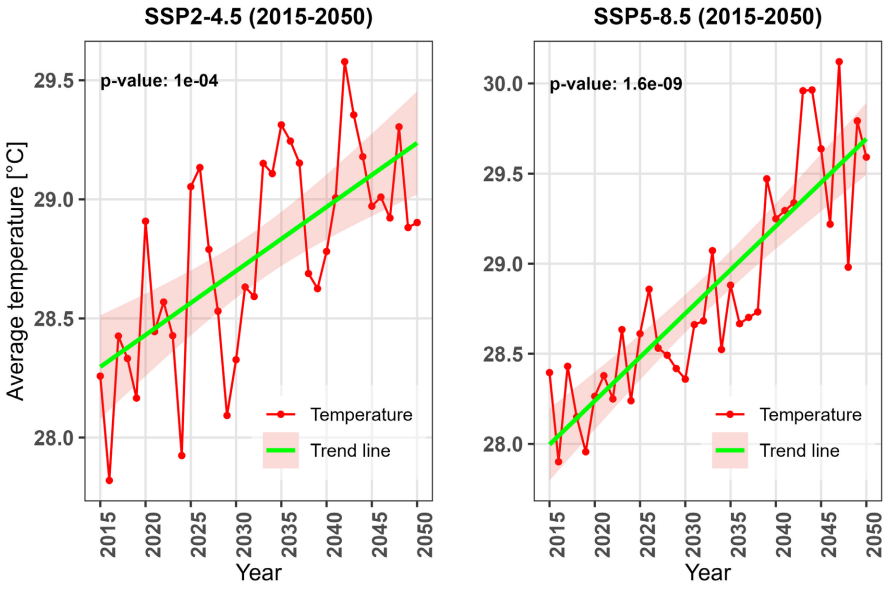

Figure 5. Average temperature trend over the projection period (left: SSP2-4.5 scenario, right: SSP5-8.5 scenario).

Table 5. Comparison of Theil-Sen slope results.

Variable	Season	Reference Slope	SSP2-4.5		SSP5-8.5	
			Slope	ΔX	Slope	ΔX
Rainfall [mm/year]	DJF	0.05	0.00	−0.05	0.01	−0.04
	MAM	0.33	2.44	2.11	1.51	1.18
	JJA	0.40	4.23	3.83	1.83	1.43
	SON	1.38	−1.41	−2.79	0.97	−0.41
Temperature [°C/year]	DJF	0.04	0.03	−0.01	0.05	0.01
	MAM	0.04	0.03	−0.01	0.05	0.01
	JJA	0.01	0.01	0	0.04	0.03
	SON	0.01	0.03	0.02	0.04	0.03

3.3. Breakpoint in the Data

Precipitation: analysis of the homogeneity of precipitation data over the reference period (1981-2014) using the Pettitt test reveals continuity in the mean. The series therefore shows no breaks. The null hypothesis (H_0) assumes the existence of a

break in the mean within the series, while the alternative hypothesis (H_1) assumes the absence of a break in the mean. As the p-value obtained (0.176) is greater than the 5% significance threshold, the null hypothesis is rejected in favor of the alternative hypothesis. This result indicates the absence of a significant break in the mean, with a 17.6% risk of error. It is therefore accepted that there is no break in the reference series data. The same is true for the SSP2-4.5 scenario, where the p-value of 0.069 is greater than 0.05. It is therefore concluded that for the SSP2-4.5 scenario, there is no break in the data series. For the SSP5-8.5 scenario, the test reveals a break in the mean with a p-value of 0.023, which is below the 5% significance threshold. In the average annual precipitation data, the break is observed in 2035, as shown in **Figure 6**. The average before the break is 1170.96 mm compared to 1275.14 mm. The series is therefore inhomogeneous. The break observed in the series could be due to several factors, such as sensor measurement errors or climatic factors [49].

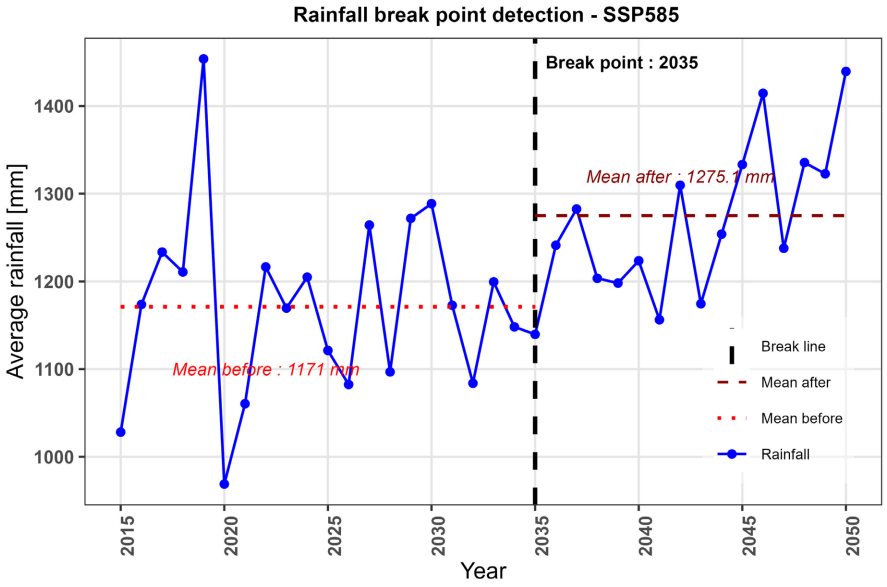

Figure 6. Break in the SSP5-8.5 scenario rainfall data.

Temperature: analysis of the homogeneity of precipitation data over the reference period (1981-2014) and projection period (2015-2050) using the Pettitt test reveals a discontinuity in the mean in each of the series. The test hypotheses remain the same as those formulated for precipitation. The p-values calculated for the reference scenarios, SSP2-4.5 and SSP5-8.5, are 0.042, 0.0002, and 1.761×10^{-5} respectively, all of which are below the significance threshold set at 5%. The null hypothesis is therefore accepted for each of the scenarios. It is therefore concluded that for each of these emission scenarios, there is a break in the data series (**Figure 7**). The breaks are identified in 1995, 2032, and 2031, with changes in the mean of around 0.42˚C (reference scenario), 0.62˚C (SSP2-4.5 scenario), and 0.82˚C (SSP5-8.5 scenario), as shown in **Figure 7** and **Figure 8**. For the reference period, the average before the break is 27.4˚C compared to 27.8˚C. The series is therefore

inhomogeneous. These will provide a better explanation of climate behavior and, consequently, of normal values.

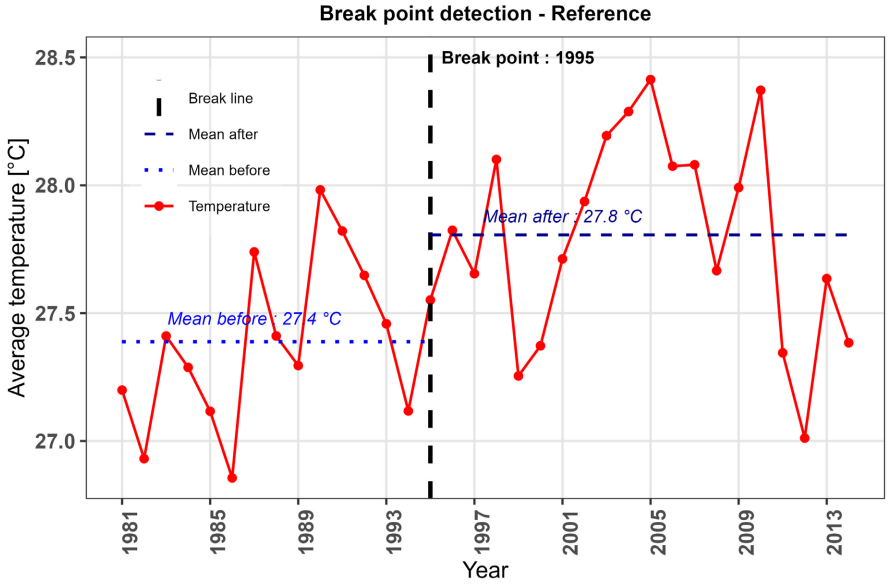

Figure 7. Break in the reference temperature data.

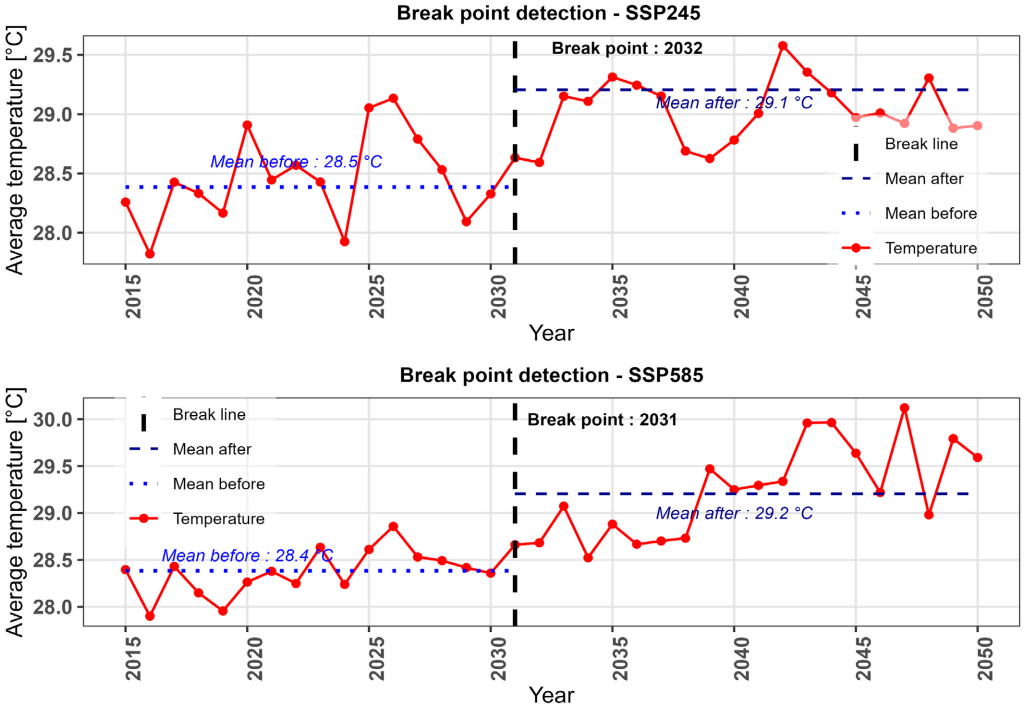

Figure 8. Breaks in SSP2-4.5 and SSP5-8.5 temperature projection data.

3.4. Climate Normal

Normals serve as a reference against which recent or current observations can be compared. They are also widely used, implicitly or explicitly, to determine the conditions that can be most expected in a given location [38]. In this study, dif-

ferent normals were calculated for both precipitation and temperature. The norms evaluated include the 1991-2020 norms currently in use (reference norm) as well as the future 2001-2030, 2011-2040, and 2021-2050 normals. The following Figures show the evolution of the norms relative to the reference norm for the SSP2-4.5 and SSP5-8.5 scenarios.

Precipitation normals: the assessment of normals using the SSP2-4.5 scenario shows an increase in annual precipitation at each of the stations in the basin. However, Figure 9 shows that the northern part of the basin could experience an increase in precipitation at the Orodara, Samoroguan, virtual 7, and virtual 8 stations. At these stations, an upward trend in climate normals is observed, while the other stations also show an upward trend specific to their local characteristics. The Mouhoun watershed in Samandeni, located in the Sudanese phytogeographic zone of Burkina Faso, is characterized by annual rainfall exceeding 900 mm according to the climate norm established by ANAM.

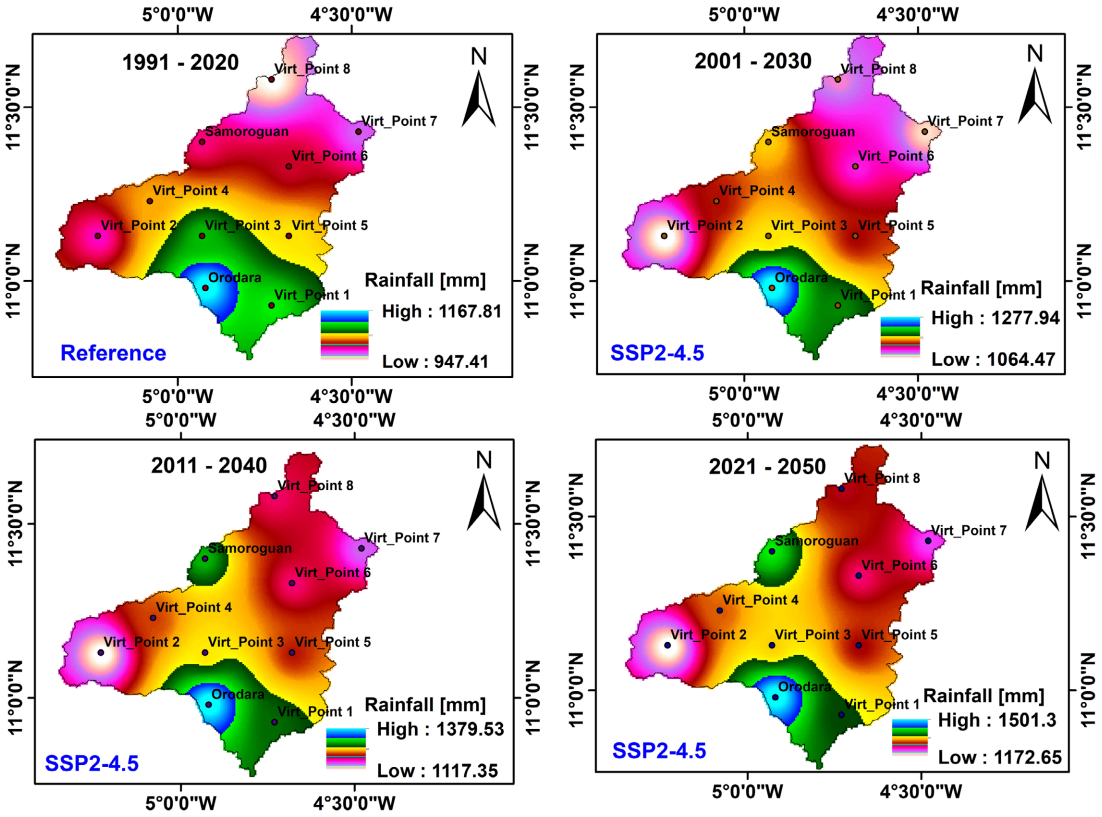

Figure 9. Changes in precipitation norms according to the SSP2-4.5 scenario.

For the 1991-2020 norm, three climate sub-area emerge:

1) Sub-area 1: $P_{ann} < 1\,000$ mm,

2) Sub-area 2: 1000 mm $< P_{ann} < 1100$,

3) Sub-area $P_{ann} > 1100$ mm.

Results of the classification of these normals by sub-zone for the SSP2-4.5 scenario are shown in Table 6.

Table 6. Climate sub-area by precipitation normals according to the SSP2-4.5 scenario

Normals	Sub area	Rainfall range (mm)
2001-2030	I	$P_{ann} < 1110$
	II	$1110 < P_{ann} < 1180$
	III	$P_{ann} > 1180$
2011-2040	I	$P_{ann} < 1180$
	II	$1180 < P_{ann} < 1260$
	III	$P_{ann} > 1260$
2021-2050	I	$P_{ann} < 1180$
	II	$1110 < P_{ann} < 1340$
	III	$P_{ann} > 1340$

where

P_{ann} is the average annual precipitation recorded at the station.

The norms derived from the SSP5-8.5 scenario (Figure 10) follow the same pattern as those from the SSP2-4.5 scenario.

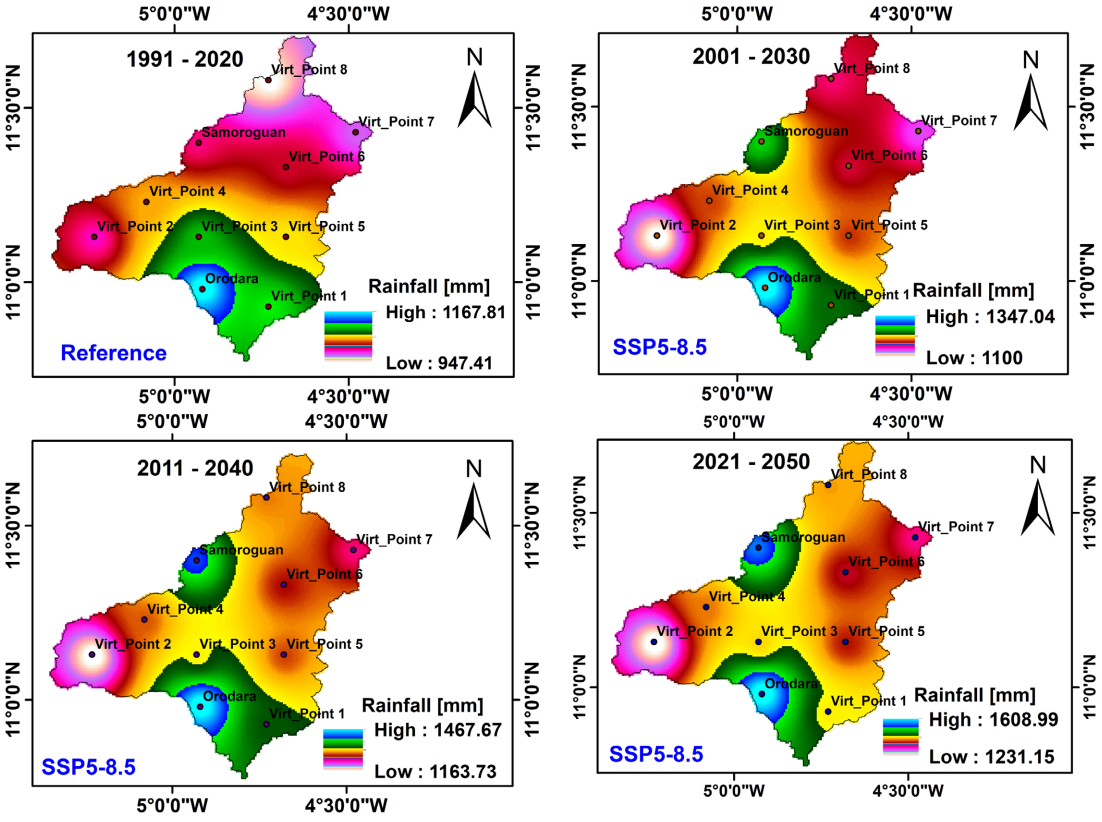

Figure 10. Change in precipitation normals according to the SSP5-8.5 scenario.

The normals for this emissions scenario also show three (03) main climate subzones, summarized in Table 7, where the normals show an upward trend at cer-

tain stations. For each normal, these sub-zones correspond to climate domains delimited by ranges of average annual precipitation.

Table 7. Climate sub-area by precipitation normals according to the SSP5-8.5 scenario.

Normals	Sub area	Rainfall range (mm)
2001-2030	I	$P_{ann} < 1140$
	II	$1140 < P_{ann} < 1240$
	III	$P_{ann} > 1240$
2011-2040	I	$P_{ann} < 1160$
	II	$1160 < P_{ann} < 1330$
	III	$P_{ann} > 1330$
2021-2050	I	$P_{ann} < 1235$
	II	$1235 < P_{ann} < 1550$
	III	$P_{ann} > 1550$

Oradara and Samorogouan stations could see sharp increases in annual precipitation over the years covering the different normal periods (Figure 10). According to the SSP2-4.5 and SSP5-8.5 scenarios, precipitation norms could increase across the entire watershed.

Normal temperatures: Normal temperatures vary very little. The results also show an upward trend in normal temperatures. The western part of the basin could experience a greater increase in temperatures (Figure 11). This warming could spread from the western to the eastern part of the basin. According to the SSP2-4.5 emissions scenario, this spread could lead to a significant increase in temperature in the corridor encompassing the Samoroguan station and the virtual stations at grid bridge 2, point 3, point 4, and point 6 of the watershed. Overall, for this emission scenario, and based on the 2001-2030 to 2021-2050 normals, the low average temperatures in the northern and southern parts of the basin could evolve to reach, in the western part, the highest temperatures of the 1991-2020 normal (28.2˚C) over the watershed.

The analysis of the SSP5-8.5 scenario is also consistent with the SSP2-4.5 emissions scenario (Figure 12), with the same propagation direction (west-east). According to this scenario, the average temperature of the watershed over the 2021-2050 normal period could approach that of the 1991-2020 normal period. Furthermore, based on the 2001-2030 and 2011-2040 normals, the low average temperatures in the northern and southern parts of the basin could evolve to reach the highest temperatures in the western part (28.2˚C) of the basin based on the 1991-2020 normal.

Overall, temperatures for the various normals derived from the SSP2-4.5 and SSP5-8.5 scenarios could increase across the entire watershed.

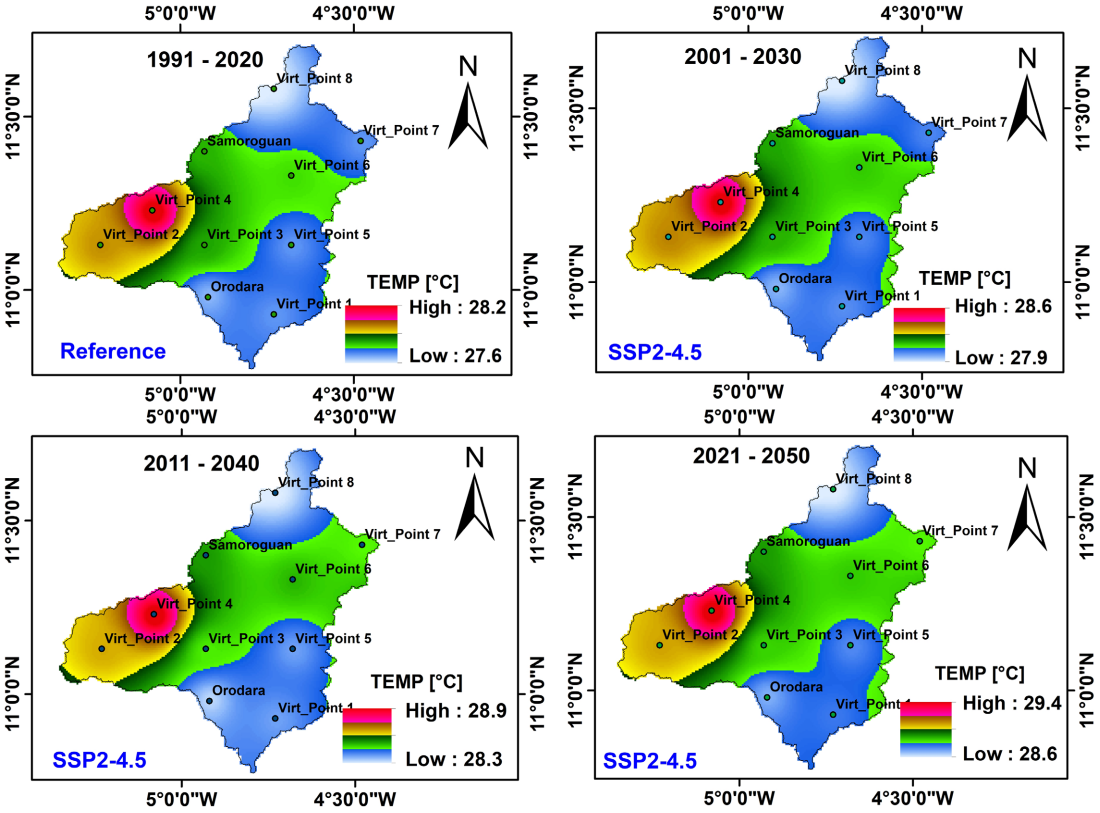

Figure 11. Temperature data spatialization according to the SSP2-4.5 scenario.

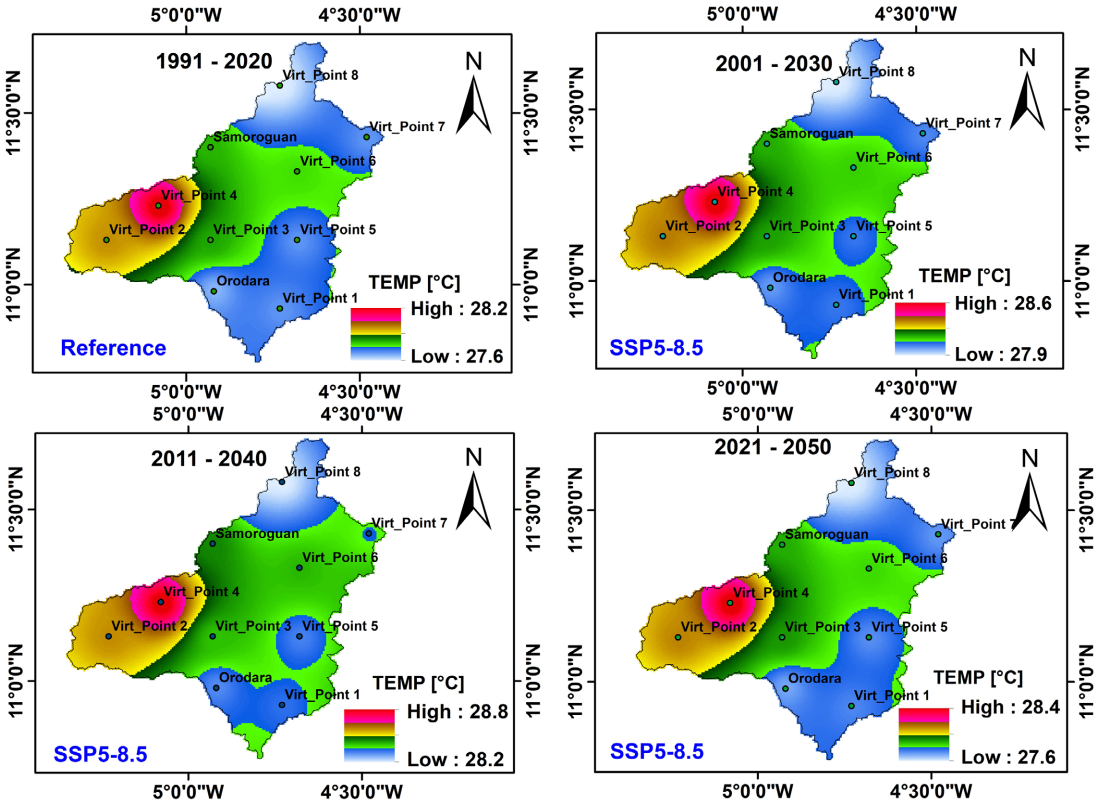

Figure 12. Temperature data spatialization according to the SSP5-8.5 scenario.

3.5. Precipitation Index

The results of the analysis of precipitation index trends selected for the study (CWD, CDD, SDII, and RX1day) over the reference period are presented in Figure 13. Over the reference period, the results of applying the Mann-Kendall test to these indices show that for:

- SDII: the trend is negative and statistically significant with a p-value of 0.046 above the 5% significance threshold; a slope of −0.036 mm/day, and a negative Z statistic of −1.986,
- CWD: the trend is positive and non-significant with a p-value of 0.091 above the 5% significance threshold. The Sen slope is 0.15 days against a positive Z statistic of 1.687. The number of wet days varies between 7 and 24 days for rainy days (precipitation greater than 1 mm),
- CDD and RX1day all have a negative trend that is non-significant, with p-values of 0.246 and 0.812 respectively, both above the 5% significance threshold, Z statistics of −1.158 and −0.237 respectively, both negative, and slopes of −0.24 days and −0.639 mm respectively.

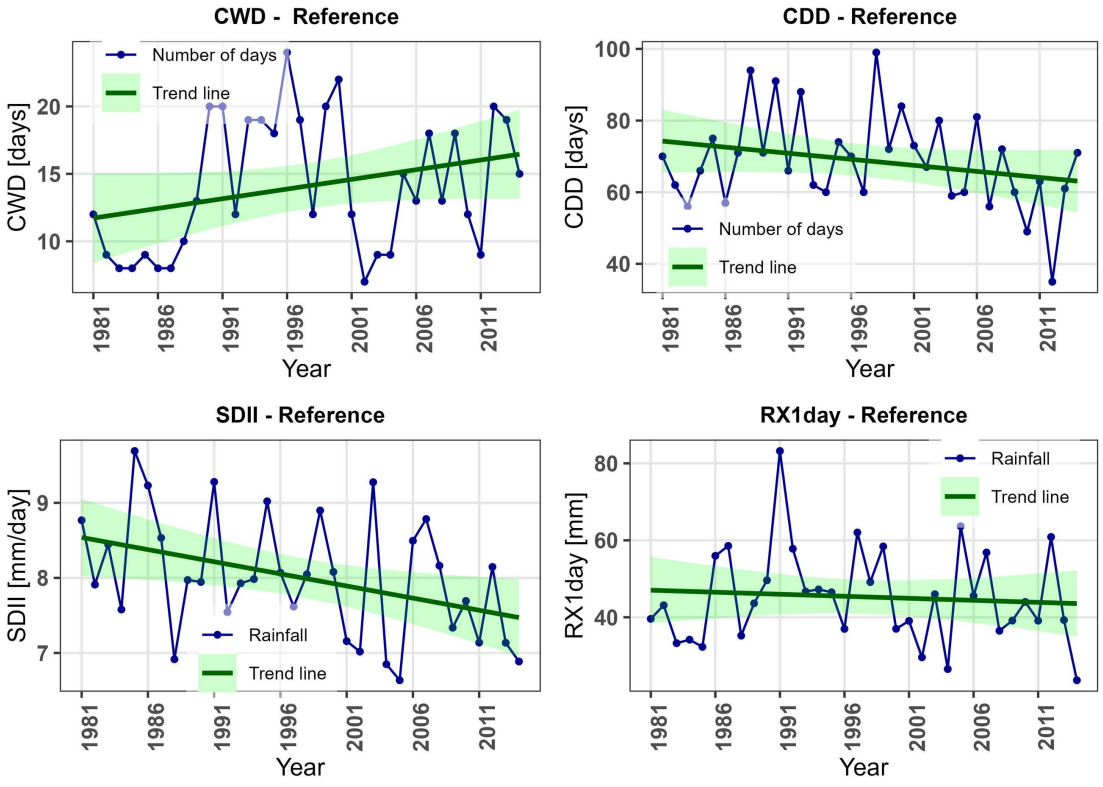

Figure 13. Trends in the CWD, CDD, SDII, and RX1day climate indices over the reference period.

Over the projection period, the results of applying the Mann–Kendall test to these indices for the SSP2-4.5 scenario show that:

- The SDII index has a significant positive upward trend, while the RX1day index has a non-significant upward trend (Figure 14). The SDII index has a p-value of 0.048, which is below the 5% significance threshold, while the RX1day

index has a p-value of 0.105, which is above the 5% significance threshold. These indices have Mann-Kendall Z statistics of 1.975 and 1.62, respectively, both of which are positive; slopes of 0.021 mm/day and 0.119 mm, respectively;

- As for the CWD and CDD indices, they all show a non-significant downward trend with respective p-values of 0.924 and 0.353, both above the 5% significance threshold, respective Z statistics of −0.095 and −0.928, both negative, and respective slopes of zero and −0.155 day.

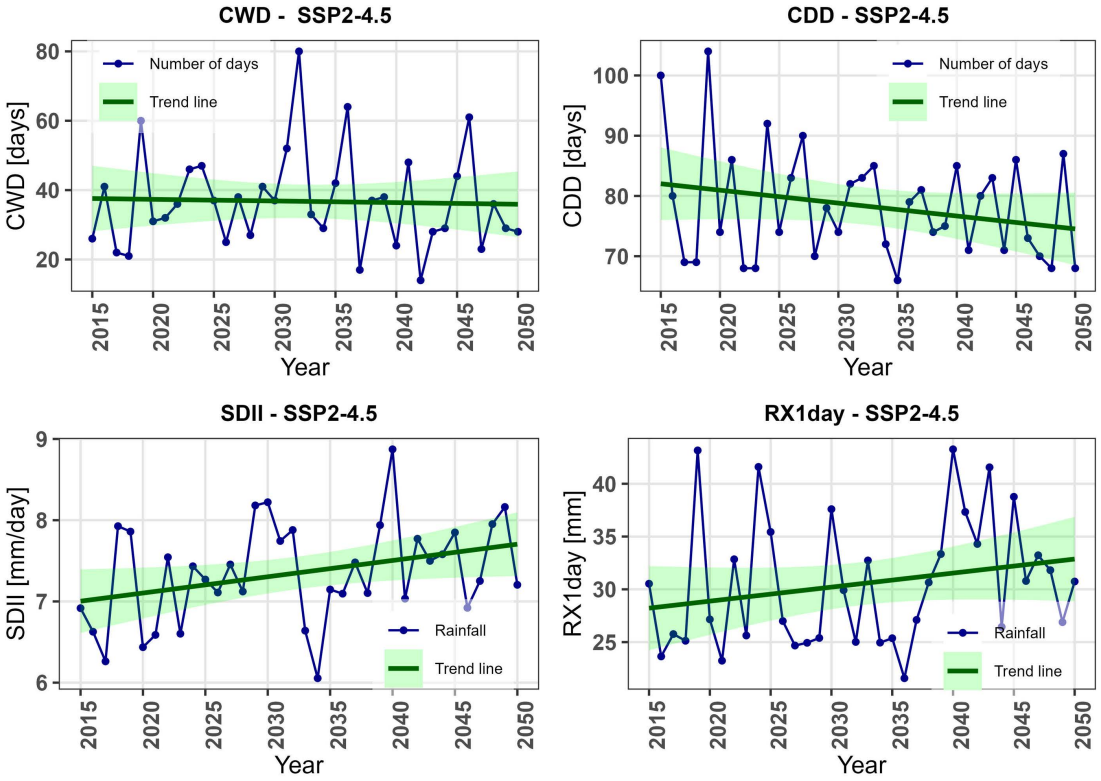

Figure 14. Trends in the CWD, CDD, SDII, and RX1day climate indices over the SSP2-4.5.

For SSP5-8.5, the results of applying the Mann–Kendall test show (**Figure 15**) that:

- CWD, SDII, and RX1day all have positive trends with non-significance. The p-values are 0.87, 0.32, and 0.692, respectively, all above the 5% significance threshold. The Z statistics obtained are 0.163, 0.994, and 0.395, respectively, all positive. The slopes obtained are 0.04 days, 0.012 mm/day, and 0.041 mm, respectively.
- The CDD shows a non-significant downward trend with a p-value of 0.088 above the significance threshold, a negative Z-statistic of −1.705, and a slope of −0.267 days.

3.6. Temperature Index

In this section, trends in the TXx and TNn temperature indices were studied over the reference period (**Figure 16**) and over the projection period, particularly with the SSP2-4.5 (**Figure 17**) and SSP5-8.5 (**Figure 18**) scenarios.

- The TXx indices for the periods 1981-2014 (Figure 16) and 2015-2050 all show statistically significant positive trends. The p-value obtained for the reference period is 7.37×10^{-7}, compared to 4.19×10^{-4} and 9.26×10^{-5} for SSP2-4.5 and SSP5-8.5, respectively (Figure 17 and 18). The Z-statistic is 4.951 for the reference period, 3.527 and 3.909 for SSP2-4.5 and SSP5-8.5, respectively. The slopes

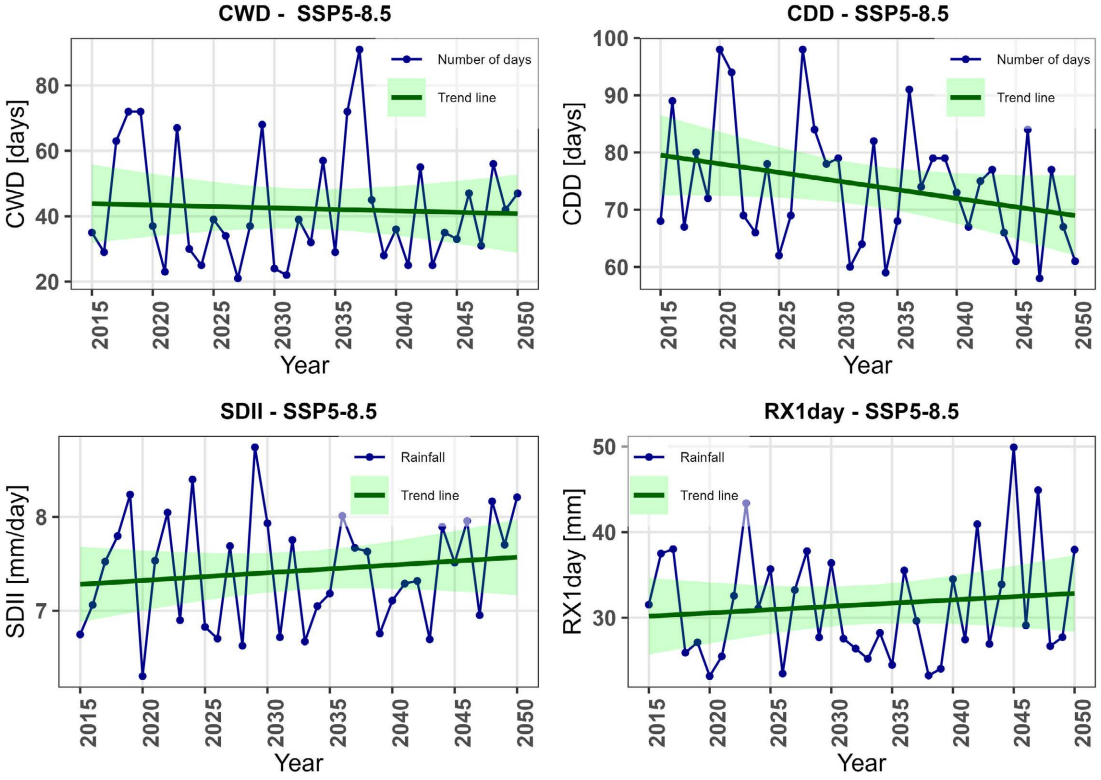

Figure 15. Trends in the CWD, CDD, SDII, and RX1day climate indices over the SSP5-8.5.

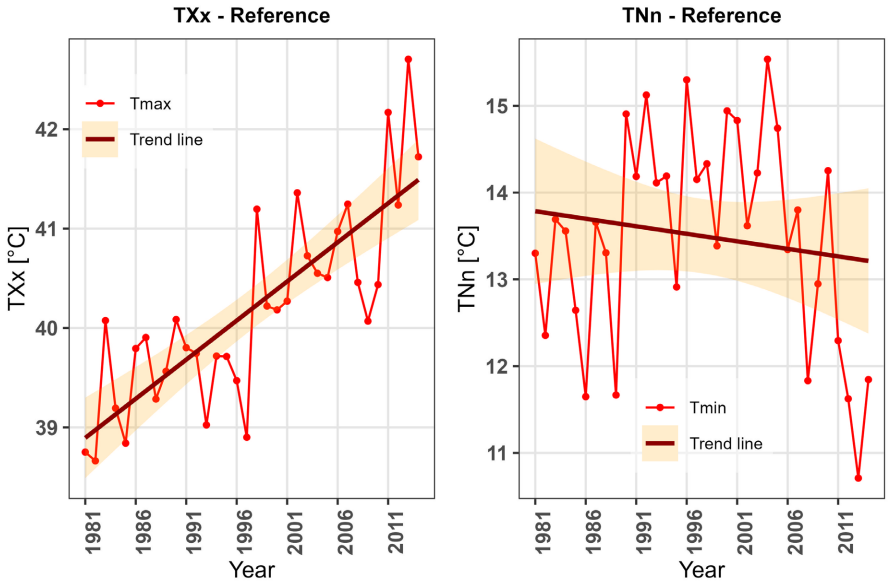

Figure 16. Trends in the TXx and TNn climate indices over the reference period.

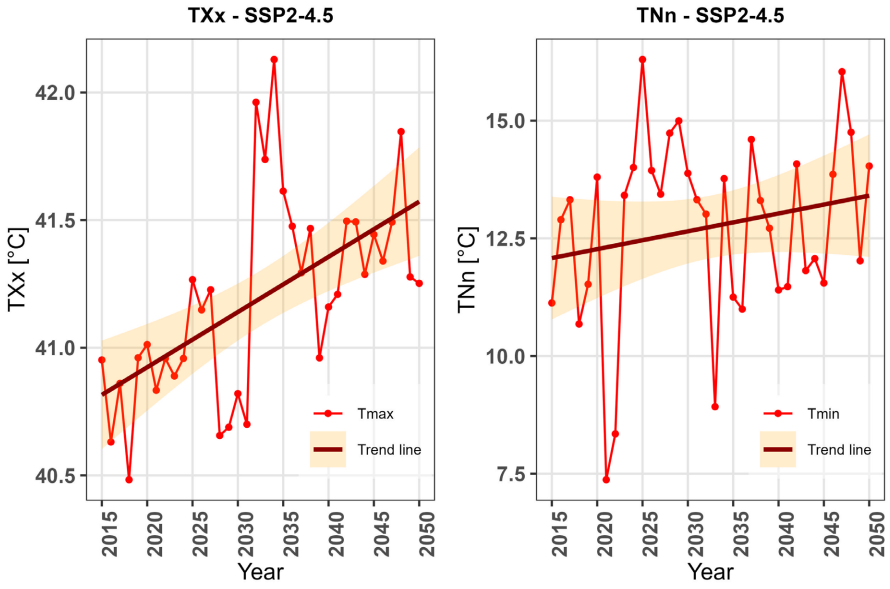

Figure 17. Trends in the TXx and TNn climate indices for the SSP2-4.5 scenario.

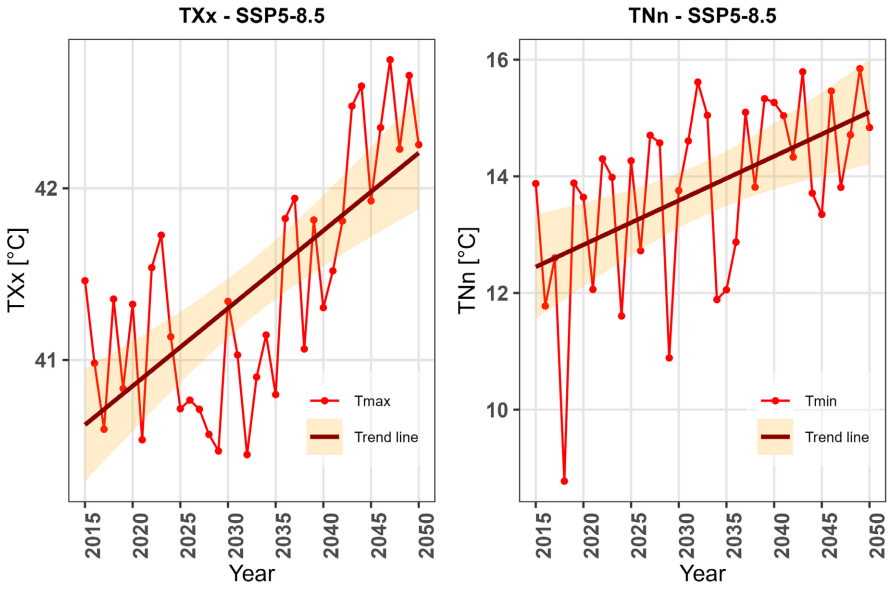

Figure 18. Trends in the TXx and TNn climate indices for the SSP5-8.5 scenario.

are 0.077˚C/year for the reference period and 0.027˚C/year and 0.045˚C/year for SSP2-4.5 and SSP5-8.5, respectively.

- The TNn index over the reference period shows a non-significant negative trend (Figure 16) with a p-value of 0.789 relative to the 5% significance threshold, a negative Z-statistic of −0.266, and a slope of −0.0008˚C/year. For the SSP2-4.5 scenario, the trend is positive but not significant, with a p-value of 0.281 relative to the 5% significance threshold. The Z-statistic indicates a positive value of 1.0761. The slope is 0.077˚C/year for SSP2-4.5 and SSP5-8.5. However, scenario SSP5-8.5 indicates a significant upward trend, reflected in a p-value of 0.00124, which is below the 5% threshold considered to be the signif-

icance threshold. A positive Z-statistic of 3.228 with a slope of 0.065˚C/year.

4. Discussion

4.1. Inter-Model Uncertainty

The choice of the CanESM5 model from among 27 models in the CMIP6 project is motivated by several factors supported by recent scientific literature on West Africa. At the West African scale, comparative analyses of CMIP6 models show significant variability in model performance depending on climate variables. This variability is all the greater given that, in West African regions and sub-regions, precipitation simulation is linked to the West African monsoon [50] [51]. Several studies indicate that the multi-model average does not necessarily guarantee an improvement in regional climate representation, particularly when certain models exhibit marked systematic biases. that is to say, the usual model combination approach of applying an overall weighting to the models can dilute the accuracy of regional forecasts [4] [52] [53]. In this context, the use of a well-evaluated individual model may be scientifically more relevant than a multi-model approach. Moreover, in the work of [54], it appears that the CanESM5 model is cited as one of the best models with good performance after bias correction for simulating historical precipitation.

Recent studies focusing on West Africa and the Sahel show that certain individual CMIP6 models, including CanESM5, satisfactorily reproduce the seasonal precipitation cycle, interannual variability, and historical trends when compared to observations [2]. In addition, CanESM5 has a large set of simulations, allowing for a better characterization of internal climate variability, which is a dominant source of uncertainty at the regional and hydrological scales. For Burkina Faso in general, and the Mouhoun basin in particular, where precipitation patterns are strongly controlled by convective processes and monsoon dynamics, the use of a single, physically consistent, and well-evaluated model is therefore considered sufficient and methodologically appropriate for the objectives of the study.

The results of the inter-model analysis show significant inter-model disagreement regarding the amplitude of simulated precipitation. These results are consistent with the work of [44], which shows that, despite the improvements made by CMIP6 models, precipitation projections in West Africa remain characterized by high inter-model uncertainty. Although the uncertainty is high, there is relative consensus among the majority of models. Furthermore, [55] [56] report that for precipitation projections, climate models show strong disagreements, ranging from much wetter to much drier future conditions.

4.2. Model Comparison Analysis

A comparison of CanESM5 with the multi-model median for the period 1981-2014 shows that, for the Mouhoun basin in Samandeni, CanESM5 has an average bias of 74.5% compared to the median of the 27 CMIP6 models (PBIAIS = 74.5%, ME = 1.2; RMSE = 3.78 and RSD = 1.68). This bias shows that CanESM5 is not

broadly representative of the multi-model trend for the basin. However, a comparison of the CanESM5 model with observations, despite its difference from the multi-model median, shows that CanESM5 better reproduces the observed precipitation in the Mouhoun basin (PBIAS = 1.8%, ME = 0.05, RMSE = 6.13 and RSD = 0.77), making it appropriate for analysis at the scale of the Mouhoun watershed in Samandeni. The results of the comparison of the multi-model median with observations (PBIAS = 71.5%, ME = 1.15; RMSE = 5.56 and RSD = 2.18), confirm the relevance of choosing CanESM5. The results based on the CanESM5 model must be interpreted taking into account the deviation from the multi-model median, which reflects the structural uncertainty between models.

Furthermore, in the context of climate sensitivity, it should be noted that the most recent version of the Canadian Earth System Model (CanESM5.0.3) is distinguished by an effective climate sensitivity (EffCS) estimated at 5.65 K. This value is the highest among the CMIP6 models [57]. According to [58] [59], the main factors contributing to the increased climate sensitivity of CanESM5 are more positive feedbacks from low and non-low shortwave clouds, particularly with respect to low clouds in the equatorial Pacific, as well as the optical depth of clouds in the subtropical and extratropical free troposphere. This high equilibrium climate sensitivity implies an amplified response of the simulated climate system to the radiative forcings imposed by the SSP scenarios, resulting in more pronounced projected trends in the analyzed climate variables.

4.3. Changes in Precipitation and Temperature

The results of this study show that precipitation and temperatures are increasing in the Mouhoun watershed in Samandeni. These results confirm those of [60] according to which the temporal evolution of temperatures shows an upward trend in the main climatic regions of Burkina Faso. Other studies, such as those by [10] which show an upward trend in temperature in the Djôrô region (formerly Southwest) in the Sudanese domain. This upward trend in precipitation could promote the recurrence of increasingly intense rainfall, thereby increasing the risk of extreme events, particularly flooding. To this end, [61] emphasizes that the intensity and frequency of heavy rainfall have increased in recent decades in almost all regions of Burkina Faso. This could significantly affect agricultural yields by disrupting the growth cycle of plants, leading to food insecurity. Rising temperatures could affect crop cycles, causing plants to wilt, yields to decline, and a transition to agriculture that is more resilient to the effects of temperature variation [62] [63] [64]. The implications for rain-fed agriculture, water management, and warning systems are significant: delayed planting, more frequent intras seasonal droughts, and increased water stress [65]. Indeed, heat stress significantly reduces yields of essential food crops. Crops such as wheat (Triticum aestivum), rice (Oryza sativa), corn (Zea mays), soybeans (Glycine max), sorghum (Sorghum bicolor), sugarcane (Saccharum officinarum), tomatoes (Solanum lycopersicum), and common beans (Phaseolus vulgaris) experience yield losses estimated at between 3% and 10% for

every 1˚C increase above 30˚C [66]-[68].

According to the SSP2-4.5 scenario, average annual precipitation could reach 1160 mm/year (normal 2001-2030), 1380 mm/year (normal 2011-2040), and 1500 mm/year (normal 2021-2050). However, according to the SSP5-8.5 scenario, average annual precipitation could reach 1345 mm/year (normal 2001-2030), 1460 mm/year (normal 2011-2040) and 1600 mm/year (normal 2021-2050). Compared to the current normal (1991-2020), where average annual precipitation does not exceed 1168 mm, the watershed could experience an increase in rainfall for both the SSP2-4.5 and SSP5-8.5 scenarios.

This analysis clearly shows that the climate norm is shifting increasingly towards the northern part of the watershed, with the southern part likely to become increasingly humid. In addition, the seasonal analysis shows that the rainy season extends even further into the MAM, JJA, and SON seasons in the Mouhoun watershed in Samandeni. It should be noted that this study does not address the start and end dates of the season, but provides a brief overview of the spread of the season over the Mouhoun watershed in Samandeni. These results are consistent with those of [10] [69] according to which the rainy season begins before the end of May and ends before the end of October in the Sudanese zone of Burkina Faso. The increasing trend in temperature norms in the basin according to the two scenarios clearly shows that temperatures could rise in the Mouhoun watershed in Samandeni. Such an increase in temperature could lead to evaporation of water bodies, particularly the Samandeni dam. It could also disrupt the plant development cycle and consequently affect crop yields, especially in a watershed such as Mouhoun in Samandeni, where agricultural practices are extensive. The impacts are not limited to agriculture; they also affect hydroelectricity, which is heavily dependent on water from the dam. Furthermore, according to [70], by 2050, the increase in extreme rainfall will cause the worst decline in agricultural yields in the western regions of the country, namely 27%, 24% and 23% in the regions of Tannounyan (formerly the Cascades region), Djôrô (formerly the Southwest) and Guiriko (formerly the Hauts-Bassins) respectively. These results confirm those of [2] [3] according to which global warming will be amplified in West Africa.

4.4. Homogeneity Analysis

Precipitation: the break observed in 2035 in the precipitation series of the SSP5-8.5 scenario can be interpreted as a temporal marker signaling the emergence of the forced signal in the projections, rather than a dynamic transition in the climate system. Its analysis is therefore based on the continuous evolution of the projected series.

Temperatures: the results obtained from applying the Pettitt test to the reference period data show a break in 1995. This leads to the series being split into two parts, i.e. 1981-1995 and 1996-2014. Although the Pettitt test detected two breaks in the temperature projection data, specifically in 2032 and 2031 for the SSP2-4.5 and SSP5-8.5 scenarios respectively, they are also interpreted as statistical indica-

tors of a gradual transition induced by anthropogenic forcing, rather than evidence of sudden changes in atmospheric circulation patterns. This clarification has been explicitly added to the manuscript to avoid any overestimation of the physical significance of the detected breaks. The analyses will therefore be based on the continuous evolution of the projected series for each scenario.

Findings are consistent with the conclusions of previous studies [71] [72] which show that, in highly forced climate projections, regime shift tests can confuse amplified trends with apparent breaks.

4.5. Climate Index

Over the period 1981-2014 (reference period), analysis of climate extremes at the watershed scale shows an increasing trend in CWD and a decreasing trend in CDD. These trends indicate wetter climatic conditions in the watershed. An increase in wet days could lead to more frequent flooding [73]. The SDII and RX1day indices, on the other hand, all show a downward trend, reflecting a decrease in maximum daily rainfall and rainfall intensity. These results are consistent with those of [74] which show that, over the period 1982-2016, the CWD index has a tendency to increase in the western Sahel, while the CDD index has a tendency to decrease in the Sahel and Sahara. The observed results of decreasing SDII and RX1day trends are contrary to those obtained in the work of [74]. This could be explained by the spatial variability of precipitation.

However, over the projection period (2015-2050), the SSP2-4.5 and SSP5-8.5 scenarios show a downward trend in CWD and CDD and an upward trend in SDII and RX1day over the watershed. Future changes in the trends of these indices could have major impacts on the frequency of droughts and floods, agricultural production, and agriculture as a whole within the basin. These results for SDII and RX1day indicate projected more intense rainfall events with an increase in maximum daily rainfall, which could increase runoff and increase the risk of flooding in the watershed. These results corroborate those of [75] which confirms a projected increase in SDII and RX1day over the period 2020-2030 at Bobo-Dioulasso synoptic station near the Mouhoun watershed in Samandeni.

Except for the TNn index over the period 1981-2014, where a downward trend is observed, the TXx and TNn temperature indices all show an upward trend over the periods 1981-2014 and 2015-2050. This reflects an increase in minimum temperatures over the period 2015-2050 for scenarios SSP2-4.5 and SSP5-8.5 and a decrease in minimum temperatures over the period 1981-2014. The results of this study corroborate those of [75] [76]. The rise in minimum and maximum temperatures will cause the watershed to warm up, which could increase evaporation in the watershed, particularly in the Samandeni dam reservoir. This increase in temperature could affect crop yields by disrupting the growth cycle of crops such as corn, millet, sorghum, and cotton grown in the watershed. The trend toward higher maximum temperatures is more significant than those toward higher minimum temperatures. This is consistent with the work of [77] which shows a more significant

increase in maximum temperatures compared to minimum temperatures.

5. Conclusion

The study highlighted changes in rainfall and temperature across the Mouhoun watershed and compared future norms with those of the reference period. Overall, the study shows that both precipitation and average annual temperatures are on the rise. According to the normals, average annual precipitation maximums could increase from 947.41 mm to 1501.3 mm for the SSP2-4.5 scenario and from 947.41 mm to 1608.99 mm for the SSP5-8.5 scenario, between the 1991-2020 normals and the 2021-2050 normals. On the other hand, maximum average annual temperatures could also rise from 27.6˚C to 28.4˚C for SSP2-4.5 and to 29.4˚C for the SSP5-8.5 scenario, between the 1991-2020 normals and the 2021-2050 normal. Analysis of the normals highlights increasingly abundant rainfall across the entire basin. The southern part of the basin will remain the wettest according to the normals, while the northern part will experience an increase in precipitation. In terms of temperatures, an increase is expected across the entire basin, with the western part being warmer than the eastern part. Visual analysis shows that the temperature increase spread from west to east. Ultimately, the analysis highlights a return of 2021-2050 temperatures to conditions close to the 1991-2020 climate reference normal. Moreover, the study includes extreme indices relevant to sectoral uses, such as the duration of consecutive dry and wet sequences (CDD and CWD), average daily rainfall intensity (SDII) and maximum daily precipitation (RX1day). The results show an increase in SDII rainfall intensity and maximum RX1day rainfall, while CWD and CDD show a downward trend. Nevertheless, it should be noted that the results presented should be interpreted with caution due to the inherent limitations of the study, in particular the use of interpolated data to compensate for the lack of available observations in the study area.

Authors Contribution

Dioviel. Dominique SOMDA: data processing, analysis, and initial drafting.
Ali. DOUMOUNIA: scientific supervision, validation, and manuscript review.

Funding

This work was carried out as part of the PRSA-BF with the support of the LAME/UJKZ laboratory.

Data Availability

- CMIP6: NASA NEX-GDDP.
- Observations: Burkina national networks.

Conflicts of Interest

The authors declare no conflicts of interest regarding the publication of this paper.

References

[1] Quenum, G.M.L.D., Nkrumah, F., Klutse, N.A.B. and Sylla, M.B. (2021) Spatiotemporal Changes in Temperature and Precipitation in West Africa. Part I: Analysis with the CMIP6 Historical Dataset. *Water*, **13**, Article 3506. https://doi.org/10.3390/w13243506

[2] Almazroui, M., Saeed, F., Saeed, S., Nazrul Islam, M., Ismail, M., Klutse, N.A.B., *et al.* (2020) Projected Change in Temperature and Precipitation over Africa from Cmip6. *Earth Systems and Environment*, **4**, 455-475. https://doi.org/10.1007/s41748-020-00161-x

[3] IPCC (2021) Climate Change 2021: The Physical Science Basis.

[4] Klutse, N.A.B., Owusu, K. and Boafo, Y.A. (2020) Projected Temperature Increases over Northern Ghana. *SN Applied Sciences*, **2**, Article No. 1339. https://doi.org/10.1007/s42452-020-3095-3

[5] Nicholson, S.E. (2013) The West African Sahel: A Review of Recent Studies on the Rainfall Regime and Its Interannual Variability. *ISRN Meteorology*, **2013**, Article ID: 453521. https://doi.org/10.1155/2013/453521

[6] Biasutti, M. (2019) Rainfall Trends in the African Sahel: Characteristics, Processes, and Causes. *WIREs Climate Change*, **10**, e591. https://doi.org/10.1002/wcc.591

[7] Alemu, M.G., Wubneh, M.A. and Worku, T.A. (2022) Impact of Climate Change on Hydrological Response of Mojo River Catchment, Awash River Basin, Ethiopia. *Geocarto International*, **38**, Article ID: 2152497. https://doi.org/10.1080/10106049.2022.2152497

[8] Noumpoa Karambiri, B.L.C. and Gansaonre, R.N. (2023) Variabilité Spatio-temporelle de la Pluviométrie dans les Zones Climatiques du Burkina Faso: Cas de Bobo—Dioulasso, Ouagadougou et Dori. *European Scientific Journal, ESJ*, **19**, 262-283. https://doi.org/10.19044/esj.2023.v19n9p262

[9] Emami, F. and Koch, M. (2019) Modeling the Impact of Climate Change on Water Availability in the Zarrine River Basin and Inflow to the Boukan Dam, Iran. *Climate*, **7**, Article 51. https://doi.org/10.3390/cli7040051

[10] Sanou, K.M. and Lompo, M. (2024) Identification des risques climatiques sur la culture du coton (*Gossypium hirsutum* l) dans la région du Sud-ouest au Burkina Faso. *Revue Internationale Dônni*, **4**, 140-156.

[11] Cannon, A.J., Sobie, S.R. and Murdock, T.Q. (2015) Bias Correction of GCM Precipitation by Quantile Mapping: How Well Do Methods Preserve Changes in Quantiles and Extremes? *Journal of Climate*, **28**, 6938-6959. https://doi.org/10.1175/jcli-d-14-00754.1

[12] Wade, C.T., Touré, O. and Diop, M. (2015) Gestion des risques climatiques: Recherche pour des futurs résilients au climat. 96 p. http://hdl.handle.net/10625/57694

[13] Atiah, W.A., Johnson, R., Muthoni, F.K., Mengistu, G.T., Amekudzi, L.K., Kwabena, O., *et al.* (2023) Bias Correction and Spatial Disaggregation of Satellite-Based Data for the Detection of Rainfall Seasonality Indices. *Heliyon*, **9**, e17604. https://doi.org/10.1016/j.heliyon.2023.e17604

[14] Döscher, R., Acosta, M., Alessandri, A., Anthoni, P., Arsouze, T., Bergman, T., *et al.* (2022) The EC-Earth3 Earth System Model for the Coupled Model Intercomparison Project 6. *Geoscientific Model Development*, **15**, 2973-3020. https://doi.org/10.5194/gmd-15-2973-2022

[15] Calvin, K., Bond-Lamberty, B., Clarke, L., Edmonds, J., Eom, J., Hartin, C., *et al.*

(2017) The SSP4: A World of Deepening Inequality. *Global Environmental Change*, **42**, 284-296. https://doi.org/10.1016/j.gloenvcha.2016.06.010

[16] Prajapati, R.N., Ibrahim, N. and Thapa, B.R. (2023) Climate Change Impact on Water Availability in the Himalaya: Insights from Sunkoshi River Basin, Nepal. *HydroResearch*, **6**, 279-292. https://doi.org/10.1016/j.hydres.2023.10.002

[17] Arfasa, G.F., Sekyere, E.O. and Doke, D.A. (2023) Temperature and Precipitation Trend Analysis Using the CMIP6 Model in the Upper East Region of Ghana. *All Earth*, **36**, 1-14. https://doi.org/10.1080/27669645.2023.2290966

[18] Chen, S. and Yuan, X. (2021) CMIP6 Projects Less Frequent Seasonal Soil Moisture Droughts over China in Response to Different Warming Levels. *Environmental Research Letters*, **16**, Article ID: 044053. https://doi.org/10.1088/1748-9326/abe782

[19] Wang, H., Chen, J., Xu, C., Zhang, J. and Chen, H. (2020) A Framework to Quantify the Uncertainty Contribution of GCMs over Multiple Sources in Hydrological Impacts of Climate Change. *Earth's Future*, **8**, e2020EF001602. https://doi.org/10.1029/2020ef001602

[20] Gerasu, T.S., Feyissa, T.A., Gudeta, B.G., Demissie, K. and Tesfahun, M. (2024) An Evaluation of the Africa-Cordex Regional Climate Model's Performance in Simulating Air Temperatures and Precipitation in the Melka-Wakena Catchment, Southeast Ethiopia. *Heliyon*, **10**, e40720. https://doi.org/10.1016/j.heliyon.2024.e40720

[21] Taylor, K.E. (2001) Summarizing Multiple Aspects of Model Performance in a Single Diagram. *Journal of Geophysical Research*: *Atmospheres*, **106**, 7183-7192. https://doi.org/10.1029/2000jd900719

[22] Xu, Z., Hou, Z., Han, Y. and Guo, W. (2016) A Diagram for Evaluating Multiple Aspects of Model Performance in Simulating Vector Fields. *Geoscientific Model Development*, **9**, 4365-4380. https://doi.org/10.5194/gmd-9-4365-2016

[23] Hu, Z., Chen, X., Zhou, Q., Chen, D. and Li, J. (2019) DISO: A Rethink of Taylor Diagram. *International Journal of Climatology*, **39**, 2825-2832. https://doi.org/10.1002/joc.5972

[24] Zhou, Q., Chen, D., Hu, Z. and Chen, X. (2021) Decompositions of Taylor Diagram and Diso Performance Criteria. *International Journal of Climatology*, **41**, 5726-5732. https://doi.org/10.1002/joc.7149

[25] Mendez, M., Maathuis, B., Hein-Griggs, D. and Alvarado-Gamboa, L. (2020) Performance Evaluation of Bias Correction Methods for Climate Change Monthly Precipitation Projections over Costa Rica. *Water*, **12**, Article 482. https://doi.org/10.3390/w12020482

[26] Tong, Y., Gao, X., Han, Z., Xu, Y., Xu, Y. and Giorgi, F. (2020) Bias Correction of Temperature and Precipitation over China for RCM Simulations Using the QM and QDM Methods. *Climate Dynamics*, **57**, 1425-1443. https://doi.org/10.1007/s00382-020-05447-4

[27] Taïbi, S., Anza, F.Z.H. and Zeroual, S. (2021) Etude de l'impact des changements climatiques sur la disponibilité des ressources en eau basée sur les simulations du modèle climatique régional RCA4: Cas du bassin de Ain DALIA (Algérie). *Algérian Journal of Environnemental Science and Technology*, **7**, 1860-1869.

[28] Gudmundsson, L., Bremnes, J.B., Haugen, J.E. and Engen-Skaugen, T. (2012) Technical Note: Downscaling RCM Precipitation to the Station Scale Using Statistical Transformations—A Comparison of Methods. *Hydrology and Earth System Sciences*, **16**, 3383-3390. https://doi.org/10.5194/hess-16-3383-2012

[29] Kendall, M. (1975) Rank Correlation Methods. Charles Griffin.

[30] Hamed, K.H. (2008) Trend Detection in Hydrologic Data: The Mann-Kendall Trend Test under the Scaling Hypothesis. *Journal of Hydrology*, **349**, 350-363. https://doi.org/10.1016/j.jhydrol.2007.11.009

[31] Sen, P.K. (1968) Estimates of the Regression Coefficient Based on Kendall's Tau. *Journal of the American Statistical Association*, **63**, 1379-1389. https://doi.org/10.1080/01621459.1968.10480934

[32] Yacoub, E. and Tayfur, G. (2018) Trend Analysis of Temperature and Precipitation in Trarza Region of Mauritania. *Journal of Water and Climate Change*, **10**, 484-493. https://doi.org/10.2166/wcc.2018.007

[33] Yu, P., Yang, T. and Wu, C. (2002) Impact of Climate Change on Water Resources in Southern Taiwan Region. *Journal of Hydrology*, **260**, 161-175. https://doi.org/10.1016/s0022-1694(01)00614-x

[34] Irannezhad, M., Marttila, H., Chen, D. and Kløve, B. (2016) Century-Long Variability and Trends in Daily Precipitation Characteristics at Three Finnish Stations. *Advances in Climate Change Research*, **7**, 54-69. https://doi.org/10.1016/j.accre.2016.04.004

[35] Gutiérrez-Hernández, O. and García, L.V. (2024) Robust Trend Analysis in Environmental Remote Sensing: A Case Study of Cork Oak Forest Decline. *Remote Sensing*, **16**, Article 3886. https://doi.org/10.3390/rs16203886

[36] Kocsis, T., Kovács-Székely, I. and Anda, A. (2019) Homogeneity Tests and Non-Parametric Analyses of Tendencies in Precipitation Time Series in Keszthely, Western Hungary. *Theoretical and Applied Climatology*, **139**, 849-859. https://doi.org/10.1007/s00704-019-03014-4

[37] Teferi, G., Hailu, H. and Beza, M. (2025) Integrating SWAT-WEAP Models for Surface Water Availability and Demand Analysis in Gumara Watershed, Upper Blue Nile Basin, Ethiopia. *Applied and Environmental Soil Science*, **2025**, Article ID: 5546678. https://doi.org/10.1155/aess/5546678

[38] OMM (2011) Guides des pratiques climatologiques. 152 p.

[39] Koycegiz, C. and Buyukyildiz, M. (2021) Temporal Trends of Extreme Precipitation and Temperature Indices. *International Conference on Engineering Technologies* (*ICENTE*'21), Konya, 18-21 November 2021, 570-574.

[40] Xue, X., Hou, S. and Meng, C. (2023) Spatial-Temporal Variations in Temperature and Precipitation Extremes during 1960-2019 in Guizhou Province, China. *Atmosphere*, **14**, Article 1162. https://doi.org/10.3390/atmos14071162

[41] Zhao, C., Gong, J., Wang, H., Wei, S., Song, Q. and Zhou, Y. (2020) Changes of Temperature and Precipitation Extremes in a Typical Arid and Semiarid Zone: Observations and Multi-Model Ensemble Projections. *International Journal of Climatology*, **40**, 5128-5153. https://doi.org/10.1002/joc.6510

[42] Alavinia, S.H. and Zarei, M. (2020) Analysis of Spatial Changes of Extreme Precipitation and Temperature in Iran over a 50-Year Period. *International Journal of Climatology*, **41**, E2269-E2289. https://doi.org/10.1002/joc.6845

[43] Rouamba, S., Yameogo, J., Sanou, K., Zongo, R. and Yanogo, I.P. (2023) Trends and Variability of Extreme Climate Indices in the Boucle Du Mouhoun (Burkina Faso). *GEOREVIEW*, **33**, 70-84. https://doi.org/10.4316/georeview.2023.01.07

[44] Romanovska, P., Gleixner, S. and Gornott, C. (2023) Climate Data Uncertainty for Agricultural Impact Assessments in West Africa. *Theoretical and Applied Climatology*, **152**, 933-950. https://doi.org/10.1007/s00704-023-04430-3

[45] Nijsse, F.J.M.M., Cox, P.M. and Williamson, M.S. (2020) Emergent Constraints on Transient Climate Response (TCR) and Equilibrium Climate Sensitivity (ECS) from

Historical Warming in CMIP5 and CMIP6 Models. *Earth System Dynamics*, **11**, 737-750. https://doi.org/10.5194/esd-11-737-2020

[46] Forster, P.M., Maycock, A.C., McKenna, C.M. and Smith, C.J. (2019) Latest Climate Models Confirm Need for Urgent Mitigation. *Nature Climate Change*, **10**, 7-10. https://doi.org/10.1038/s41558-019-0660-0

[47] Cinkus, G., Mazzilli, N., Jourde, H., Wunsch, A., Liesch, T., Ravbar, N., *et al.* (2023) When Best Is the Enemy of Good—Critical Evaluation of Performance Criteria in Hydrological Models. *Hydrology and Earth System Sciences*, **27**, 2397-2411. https://doi.org/10.5194/hess-27-2397-2023

[48] Kambiré, G., Ouedraogo, W., Traore, D. et Somé, Y.S.C. (2023) Analyse des tendances, de la variabilité et des extrêmes climatiques dans le domaine Soudanien à l'ouest du Burkina Faso. *Djiboul*, **4**, 355-375.

[49] Shi, X., Beaulieu, C., Killick, R. and Lund, R. (2022) Changepoint Detection: An Analysis of the Central England Temperature Series. *Journal of Climate*, **35**, 6329-6342. https://doi.org/10.1175/jcli-d-21-0489.1

[50] Bichet, A., Diedhiou, A., Hingray, B., Evin, G., Touré, N.E., Browne, K.N.A., *et al.* (2020) Assessing Uncertainties in the Regional Projections of Precipitation in Cordex-Africa. *Climatic Change*, **162**, 583-601. https://doi.org/10.1007/s10584-020-02833-z

[51] Dosio, A., Jury, M.W., Almazroui, M., Ashfaq, M., Diallo, I., Engelbrecht, F.A., *et al.* (2021) Projected Future Daily Characteristics of African Precipitation Based on Global (CMIP5, CMIP6) and Regional (CORDEX, CORDEX-CORE) Climate Models. *Climate Dynamics*, **57**, 3135-3158. https://doi.org/10.1007/s00382-021-05859-w

[52] Abiodun, B.J., Mogebisa, T.O., Petja, B., Abatan, A.A. and Roland, T.R. (2019) Potential Impacts of Specific Global Warming Levels on Extreme Rainfall Events over Southern Africa in CORDEX and NEX-GDDP Ensembles. *International Journal of Climatology*, **40**, 3118-3141. https://doi.org/10.1002/joc.6386

[53] Vrac, M., Allard, D., Mariéthoz, G., Thao, S. and Schmutz, L. (2024) Distribution-based Pooling for Combination and Multi-Model Bias Correction of Climate Simulations. *Earth System Dynamics*, **15**, 735-762. https://doi.org/10.5194/esd-15-735-2024

[54] Diouf, I., Fall, P., Faye, A., Diouf, S., Diouf, A.K., Barry, M.B., *et al.* (2025) Assessment of Spatio-Temporal Trends in Rainfall Indices in Senegal: Validation of CMIP6 Models over the Historical Period and Projections under Future Climate Scenarios. *Climate*, **13**, Article 247. https://doi.org/10.3390/cli13120247

[55] Druyan, L.M. (2011) Studies of 21st-Century Precipitation Trends over West Africa. *International Journal of Climatology*, **31**, 1415-1424. https://doi.org/10.1002/joc.2180

[56] James, R., Washington, R., Abiodun, B., Kay, G., Mutemi, J., Pokam, W., *et al.* (2018) Evaluating Climate Models with an African Lens. *Bulletin of the American Meteorological Society*, **99**, 313-336. https://doi.org/10.1175/bams-d-16-0090.1

[57] Flynn, C.M. and Mauritsen, T. (2020) On the Climate Sensitivity and Historical Warming Evolution in Recent Coupled Model Ensembles. *Atmospheric Chemistry and Physics*, **20**, 7829-7842. https://doi.org/10.5194/acp-20-7829-2020

[58] Virgin, J.G., Fletcher, C.G., Cole, J.N.S., von Salzen, K. and Mitovski, T. (2021) Cloud Feedbacks from CanESM2 to CanESM5.0 and Their Influence on Climate Sensitivity. *Geoscientific Model Development*, **14**, 5355-5372. https://doi.org/10.5194/gmd-14-5355-2021

[59] Zelinka, M.D., Myers, T.A., McCoy, D.T., Po-Chedley, S., Caldwell, P.M., Ceppi, P.,

et al. (2020) Causes of Higher Climate Sensitivity in CMIP6 Models. *Geophysical Research Letters*, **47**, e2019GL085782. https://doi.org/10.1029/2019gl085782

[60] Karambiri, B.L.C.N., Dipama, J.M. and Sanou, K. (2019) Variabilité climatique et gestion efficiente de l'eau dans le bassin versant du Sourou au Burkina Faso. *Revue de Géographie de l'Université de Ouagadougou*, **1**, 65-83.

[61] Tomalka, J., Lange, S., Röhrig, F., Gornott, C., Paula, A., Chemura, A. *et al.* (2021) Profil de risque climatique: Burkina Faso. 12 p. https://www.adaptationcommunity.net/wp-content/uploads/2021/02/GIZ_Climate-risk-profile_Burkina-Faso_FR_final.pdf

[62] Kumar, A., Muthuramalingam, P., Kumar, R., Tiwari, S., Verma, L., Park, S., *et al.* (2025) Adapting Crops to Rising Temperatures: Understanding Heat Stress and Plant Resilience Mechanisms. *International Journal of Molecular Sciences*, **26**, Article 10426. https://doi.org/10.3390/ijms262110426

[63] Mahajan, S., Thakur, P., Das, S., Sharma, R.P., Manuja, S., Jha, P.K., *et al.* (2025) Impression of Contemporary Heat Stress Complexities in Agricultural Crops: A Review. *Plant Growth Regulation*, **105**, 1805-1823. https://doi.org/10.1007/s10725-025-01382-8

[64] Tran, B., Tseng, W. and Chen, C. (2025) Climate Change Impacts on Crop Yields across Temperature Rise Thresholds and Climate Zones. *Scientific Reports*, **15**, Article No. 23424. https://doi.org/10.1038/s41598-025-07405-8

[65] Sawadogo, W., Neya, T., Semde, I., Korahiré, J.A., Combasséré, A., Traoré, D.E., *et al.* (2024) Potential Impacts of Climate Change on the Sudan-Sahel Region in West Africa—Insights from Burkina Faso. *Environmental Challenges*, **15**, Article ID: 100860. https://doi.org/10.1016/j.envc.2024.100860

[66] Suzuki, N. and Mittler, R. (2005) Reactive Oxygen Species and Temperature Stresses: A Delicate Balance between Signaling and Destruction. *Physiologia Plantarum*, **126**, 45-51. https://doi.org/10.1111/j.0031-9317.2005.00582.x

[67] Agnolucci, P., Rapti, C., Alexander, P., De Lipsis, V., Holland, R.A., Eigenbrod, F., *et al.* (2020) Impacts of Rising Temperatures and Farm Management Practices on Global Yields of 18 Crops. *Nature Food*, **1**, 562-571. https://doi.org/10.1038/s43016-020-00148-x

[68] Sher, A., Noor, M.A., Li, H.X., Nasir, B., Manzoor, M.A., Hussain, S., *et al.* (2024) Heat Stress Effects on Legumes: Challenges, Management Strategies and Future Insights. *Plant Stress*, **13**, Article ID: 100537. https://doi.org/10.1016/j.stress.2024.100537

[69] Sarr, B., Kafando, L. and Atta, S. (2012) Identification des risques climatiques de la culture du maïs au Burkina Faso. *International Journal of Biological and Chemical Sciences*, **5**, 1659-1675. https://doi.org/10.4314/ijbcs.v5i4.28

[70] Schleypen, J.R., Saed, F., Dayamba, D.S., Coulibaly, J.D.O. and D'Haen, S.A.L. (2019) Impacts des changements climatiques sur l'économie (Produit intérieur brut & valeurs ajoutées sectorielles) et sur la productivité agricole au burkina faso. Climate Analytics gGmbH, 4 p.

[71] Meehl, G.A., Senior, C.A., Eyring, V., Flato, G., Lamarque, J., Stouffer, R.J., *et al.* (2020) Context for Interpreting Equilibrium Climate Sensitivity and Transient Climate Response from the CMIP6 Earth System Models. *Science Advances*, **6**, eaba1981. https://doi.org/10.1126/sciadv.aba1981

[72] Lehner, F., Deser, C., Maher, N., Marotzke, J., Fischer, E.M., Brunner, L., *et al.* (2020) Partitioning Climate Projection Uncertainty with Multiple Large Ensembles and CMIP5/6. *Earth System Dynamics*, **11**, 491-508.

https://doi.org/10.5194/esd-11-491-2020

[73] Agyekum, J., Annor, T., Quansah, E., Lamptey, B. and Okafor, G. (2022) Extreme Precipitation Indices over the Volta Basin: CMIP6 Model Evaluation. *Scientific African*, **16**, e01181. https://doi.org/10.1016/j.sciaf.2022.e01181

[74] Diatta, S., Diedhiou, C.W., Dione, D.M. and Sambou, S. (2020) Spatial Variation and Trend of Extreme Precipitation in West Africa and Teleconnections with Remote Indices. *Atmosphere*, **11**, Article 999. https://doi.org/10.3390/atmos11090999

[75] Yaméogo, H. (2025) Trends and Prediction of Extreme Precipitation Indices in Three Cities of Burkina Faso Using Non-Parametric Statistics and the Holt-Winters Smoothing Method. *Meteorology Hydrology and Water Management*, **13**, 74-103. https://doi.org/10.26491/mhwm/209088

[76] Sane, F.B. and Gaye, D. (2025) Analyse rétrospective des tendances de l'évolution récente des températures en zone côtière sénégalaise sur normale 1991-2020: Cas des stations de saint-louis et de cap skirring. *Revue Ivoirienne des Sciences et Technologie*, **45**, 166-185.

[77] Malick Ndiaye, P., Gaye, D. and Alassane Sow, S. (2020) Caractérisation Spatiotemporelle et Analyse de la Tendance des Températures au Sénégal. *European Scientific Journal, ESJ*, **16**, 105-121. https://doi.org/10.19044/esj.2020.v16n33p105